Department of Mechanical Engineering

FACULTY OF ENGINEERING AND DESIGN

FINAL YEAR MEng PROJECT REPORT

Vortex Element Modelling of Aircraft Wake Dynamic

Travis Talbot

03/04/2023

Word count: 11,140

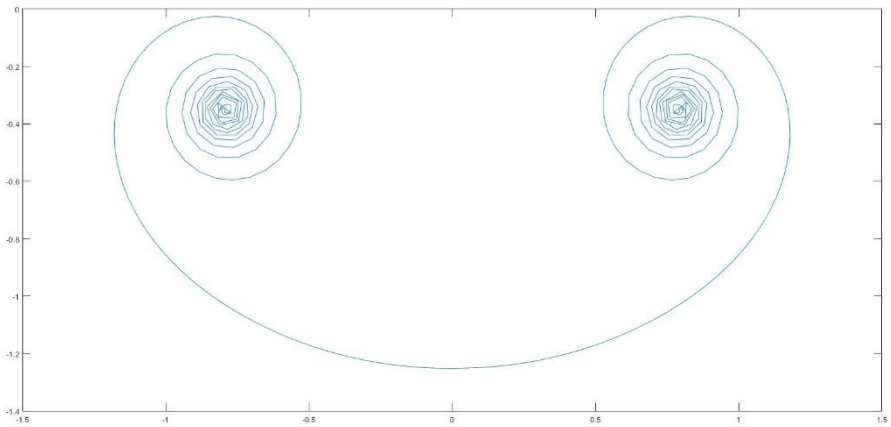

"I certify that I have read and understood the entry in the Student Handbook for the Department of Mechanical Engineering on Cheating and Plagiarism and that all material in this assignment is my own work, except where I have indicated with appropriate references."

Author's signature: Travis Talbot

Supervisor: *Michael Carley*

Assessor: *Zhijin Wang*

Vortex Element Modelling of Aircraft Wake Dynamics

Travis Talbot

Department of Mechanical Engineering

University of Bath

May 4th, 2023

Word Count: 11,140

ABSTRACT

The aim of this study was to utilise the vortex element method to create a programme that can model the rollup of the wake of an aircraft, then investigate how the discretisation of the problem effects its behaviour, if it can accurately recreate experimental results and the apply the method to a dynamic simulation of a tandem wing aircraft in pitch.

The model utilised a variation of the vortex element method developed by Robert Krasny, where the 3D flow is transformed into a 2D initial value problem where time replaces the streamwise dimension. The discretisation parameters were then subsequently investigated and it was shown that convergence of results occurred at low resolutions for the time and number of vortices in the wake, showing the model can be incredibly fast and efficient. However an additional parameter known as the smoothing factor was introduced by Krasny and this largely dictated how well the model replicated the flow, with a lower value resulting in more turns in the vortex core. However it was found that as the smoothing factor was decreased the resolution of the spatial and timesteps had to be increased to achieve a stable solution.

To assess if the method could accurately replicate the wake of a real wing, the method was used to recreate two experiments investigating the induced vertical velocity in the wake of a NACA 0012 and a NACA 0015 airfoil. This comparison showed that the VEM would achieve a similar but not fully accurate velocity profile. However, the magnitude of the velocity at the core radius was heavily dependent on the smoothing factor used and the movement of the core was not properly tracked.

Finally, a comparison was made between a dynamic and static simulation of a tandem wing aircraft pitching nose up at a set pitch rate. Results showed that the dynamic behaviour varied from the static measurements at a near constant rate and the size of this difference varied linearly with pitch rate. Showing that if the results can be validated experimentally then the dynamic behaviour in pitch will be of little concern.

CONTENTS

Abstract ii
LiSt of Figures iv
List of Figures v
Abbreviations v
1. Introduction 1
1.1. Wing Tip Vortex 1
1.2. Vortex Element Method 1
1.3. Tandem Wing Aircraft 2
1.4. Aims & Objectives 4
1.5. Report Structure 4
2. Literature Review 4
2.1. Aircraft Wake Development 4
2.1.1. Stages of Wake Development 4
2.2. Tandem Wing Aircraft 7
2.2.1. Research Methods 7
2.3. Vortex Element Method 8
3. Methodology 9
3.1. Selection of Baseline Configuration for Tandem Wing Experiment 9
3.2. Computational Methods 10
3.3. Theory 11
3.3.1. Circulation Distribution 11
3.3.2. Wake Evolution 13
3.4. Workplan 14
3.4.1. Validation of LLT and VEM Code 14
3.4.2. Sensitivity Analysis of Discretisation Parameters 15
3.4.3. Replicating Physical Flow Properties 16
3.4.4. Tandem Wing Investigation 17
4. Results 18
4.1. Analysis of Discretisation Parameters 18
4.1.1. Spatial Resolution of Vorticity Bearing Points 18
4.1.2. Timestep Analysis 20
4.1.3. Smoothing Factor Analysis – Front Wing 22
4.1.4. Smoothing Factor Analysis – Rear Wing 24
4.2. Replicating Physical Flow Properties 24
4.3. Tandem Wing Pitch Investigation 34

5. Discussion 36
6. Conclusions 37
7. References 38
8. Appendices 41
8.1. Appendix A - Classic LLT Code (LLT_1.m) 41
107.1. Appendix B – Twisted LLT Code (LLT_2_twist.m) 43
215.1. Appendix C – VEM Code (Krasny.m) 45

LIST OF FIGURES

Figure 1 - Rankine Vortex Core Model [2] 1
Figure 2 - Quickie Aircraft [7] 2
Figure 3 - Yabhon United 40 MALE UAV [9] 2
Figure 4 - Lilium Jet [11] 3
Figure 5 - 2D cross section displaying primary and secondary vortices in near field wake where Z=vertical distance, Y=distance parallel to span, C=chord length of airfoil [15] 5
Figure 6 - Passenger Aircraft Wake Rollup [30] 6
Figure 7a & 7b - Effect of stagger (7a) & gap (7b) on the sectional lift coefficient across the dimensionless span of the Fore & Hind wings 8
Figure 8(a) & 8(b) - Sectional Lift Coefficient for Twisted Wing for Comparing My Code (A) to Example Study (B) 14
Figure 9(a) & 9(B) - Wake Rollup for Comparing My Code (A) to Example Study (B) 15
Figure 10 - FIGURE 9 - EFFECT OF Number of Point Vertices On Rear Wing Total Lift Coefficient for Base Configuration 19
Figure 11a 11b & 11c - Vortex Rollup Shape for 25(a) 100(b) & 1200(c) Point Vertices 19
Figure 12 - Effect of Time Step on Rear Wing Total Lift Coefficient for Base Configuration 20
Figure 13(a) 13(b) - Effect of Time Step on Rear Wing Total Lift Coefficient for Larger Forewing from ranges 0-0.004 (A) and 0-0.1 (B) 21
Figure 14(a), 14(b), 14(c) & 14(d) - Unsteady Wake Rollup for Timestep of 0.1 After Time 0.1(a) 0.2(b) 0.3(c) & 1(d) Seconds 22
Figure 15 - Effect of SF2 on Rear Wing Total Lift Coefficient for Base Configuration 23
Figure 16(a) 16(b) 16(c) 16 (d) - The Unstable Vortex Core for SF1 = 0.005 (A), The Shape of the Wake for SF1 = 0.005 (B) SF1 = 0.05 (C) SF1 = 0.25 (D) 23
Figure 17 – Effect of SF2 on Rear Wing Total Lift Coefficient for Base Configuration 24
Figure 18 - Vortex Core For NACA 0012 Study 25
Figure 19 - Experimental Results for Vertical Velocity of NACA 0015 Wake 26
Figure 20 - VEM Vertical Velocity Centred About Experimental Core Position for NACA 0012 Study 27
Figure 21 - Zoomed VEM Vertical Velocity Centred About Experimental Core Position for NACA 0012 Study 27
Figure 22 - VEM Vertical Velocity Centred About Calculated Core Position for NACA 0012 Study 28
Figure 23 - Zoomed VEM Vertical Velocity Centred About Calculated Core Position for NACA 0012 Study 29
Figure 24 - Rollup for NACA 0015 High Resolution Study 29
Figure 25 – VEM Vertical Velocity Centred About Calculated Core Position for NACA 0015High Resolution Study 30

Figure 26 – Zoomed VEM Vertical Velocity Centred About Calculated Core Position for NACA 0015High Resolution Study 30
Figure 27 - Spanwise Displacement of Vortex Core From VEM 31
Figure 28 - Spanwise Displacement of Vortex Core From Experiment 31
Figure 29 - Vertical Displacement of Vortex Core From VEM 31
Figure 30 - Vertical Displacement of Vortex Core From Experiment 32
Figure 31 - Rollup of Vortex for NACA 0012 Study 32
Figure 32 - Experimental Results for Vertical Velocity of NACA 0012 Wake 33
Figure 33 - VEM Vertical Velocity Centred About Calculated Core Position for NACA 0012 Study 33
Figure 34 - Rear Wing Lift Coefficient Over Time for Pitch Rate of 1 deg/s 34
Figure 35 – Difference Between Static and Dynamic Rear Wing Lift Coefficient Over Time for Pitch Rate of 1 deg/s 35
Figure 36 Figure 34 - Rear Wing Lift Coefficient Over Time for Pitch Rate of 2 deg/s 35
Figure 37 - Difference Between Static and Dynamic Rear Wing Lift Coefficient Over Time for Pitch Rate of 2 deg/s 36

LIST OF FIGURES

Table 1 - Lilium Jet Dimensions [43] 10
Table 2 - Base Configuration Dimensions 10
Table 3 - Discretisation Parameters for Spatial Study 18
Table 4 - Discretisation Parameters for Timestep Study 20
Table 5 - DISCRETISATION PARAMETERS FOR SF1 Study 22
Table 6 - discretisation Parameters for SF2 Study 24
Table 7 - Parameters for NACA 0015 Study 25
Table 8 - Parameters for NACA 0012 Study 32

ABBREVIATIONS

VEM Vortex Element Method

FDM Finite Difference Method

FVM Finite Volume Method

CFD Computational Fluid Dynamics

UAV Unmanned Ariel Vehicle

e-VTOL Electric Vertical Take-off and Landing

VLM vortex lattice method

DVM discrete vortex method

1. INTRODUCTION

1.1. Wing Tip Vortex

When an aircraft moves through the air, its wings generate lift by creating a pressure differential between the upper and lower surfaces. As a result, air from the high-pressure region underneath the wing flows around the wingtip towards the low-pressure region above it, creating a pair of counter-rotating vortices. These vortices introduce a downward velocity component to the air between them known as downwash, which causes a reduction in the effective angle of attack and thus an additional induced drag force. Additionally, outwards of the vortex core an upwash is created in the opposite direction. According to the Rankine vortex model [1], the magnitude of the radial velocity of each vortex increases from zero to a maximum value between the centre point and the radius of the vortex core, beyond which it decreases as the distance from the core is increased (shown in Figure 1). The size and strength of the vortex depends on several factors including and not exclusive to wing planform, wingtip design, Reynolds number, angle of attack and atmospheric conditions.

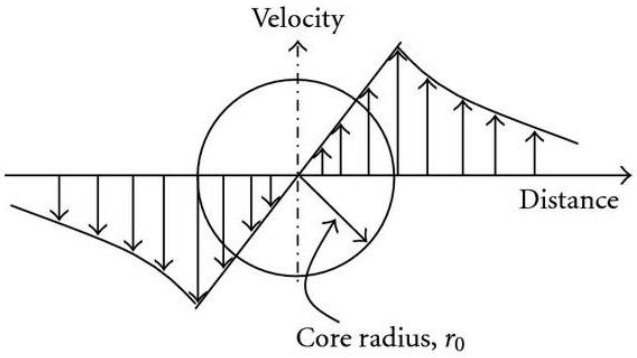

Figure 1 - Rankine Vortex Core Model [2]

It is important to understand the behaviour of an aircraft's wake as it can have severe negative implications. First, it is a key consideration in tailplane design as the downwash greatly reduces its effectiveness, making it difficult for the pilot to control the aircraft's pitch angle. To account for this, the area of the tailplane must be increased accordingly or as seen with T-tail configurations, the position must be adjusted to reduce the downwash incident on it, both of which have a negative impact on performance. In addition, the wake can cause hazardous turbulence on other aircraft that enter it, especially when the trailing aircraft is much smaller. For example, in 2017 a Bombardier Challenger temporarily lost control after an Airbus A380 passed 1,000 feet above it a minute prior, resulting in a major loss in height and some occupants sustaining serious injuries [3].

1.2. Vortex Element Method

The vortex element method (VEM) is a computational technique used to model the behaviour of incompressible fluids. It is a Lagrangian method that tracks the motion of vorticity-bearing points in the fluid, to predict the evolution of the flow field. In the VEM, the fluid is divided into many small elements and the velocity at each element is calculated based on the velocity induced by all the other elements in the fluid [4].

The VEM differs from more conventional Eulerian Computational Fluid Dynamics (CFD) methods such as the Finite Volume Method (FVM) and Finite Difference Method (FDM). Whereas FVM and FDM solve equations of fluid motion on a grid by approximating derivatives at a fixed position and time, the VEM tracks the motion of individual fluid particles over time. As such the VEM can be more computationally efficient for unsteady time dependent problems, where it can capture unsteady

effects in fewer timesteps and so is particularly effective at solving vortex dominated flows such as the wake of an aircraft. Additionally, it has shown to be particularly effective for aeroelastic problems where the airfoil cannot be rigidly fixed [5]. However, VEM is typically only valid when used to model inviscid, incompressible flow, whereas conventional CFD methods can be used to solve for a wide range of applications, including compressible and turbulent flow.

1.3. Tandem Wing Aircraft

A tandem wing aircraft is defined by having two major lifting surfaces. This differs from a canard as the main purpose of the second wing is to provide lift rather than to act as a control surface, as such the second wing will have a much greater area than a traditional canard. The advantages of this concept are a reduction in parasitic drag due to both surfaces contributing to lift, a reduced wingspan and the elimination of the tail results in a considerable reduction in aircraft length. Conversely it results in a low maximum lift coefficient due to design compromises to ensure sufficient stability and control and it is highly sensitive to changes in centre of gravity resulting in stowage problems, as well as finding it hard to balance asymmetric power in events such as engine failure [6].

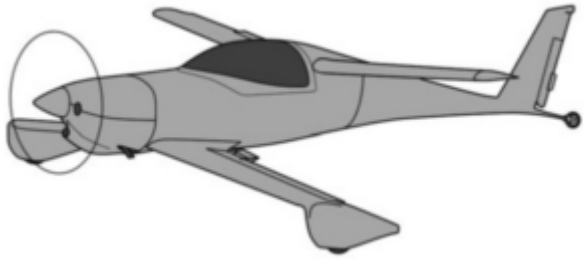

Figure 2 - Quickie Aircraft [7]

Historically the concept has seen limited usage, with the earliest concepts being poorly designed due to a lack of understanding of wing-wing interference [8]. This poor understanding led to early opinion concluding that the usage of tandem wings increases airframe mass and drag [8]. As such the scheme was not used until its re-emergence in 1977 with the creation of the Quickie homebuilt aircraft (shown in Figure 2). Now, due to its suitability to achieving high in-flight times, the concept is widely seen in many production Unmanned Ariel Vehicles (UAVs) such as the UAEs Yabhon United 40 MALE UAV (shown in Figure 3) and China's WZ-7 Soar Dragon.

Figure 3 - Yabhon United 40 MALE UAV [9]

Additionally, the recent development of Electric Vertical Take-off and Landing (e-VTOL) aircraft for urban air mobility, has provided an opportunity to utilise the tandem wing concept as a passenger

aircraft. Examples of this can be seen across a range of early concepts, with the most prominent being the Lilium jet (shown in Figure 4) which is currently undergoing flight testing [10]. The tandem wing is well suited to this application as it can offer high aspect ratios and thus superior aerodynamic performance for a limited wingspan [8]. This is highly important as to be commercially viable, these aircraft must aim to minimise their footprint to land in urban environments on infrastructure such as helipads. In addition to the aerodynamic benefits, it allows rotors to be mounted in a square configuration which provides much greater hover stability than inline rotors.

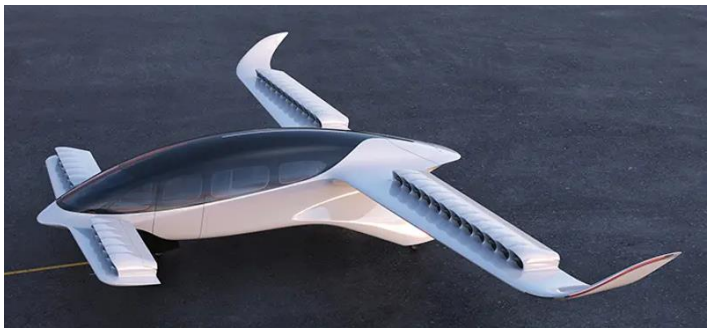

Figure 4 - Lilium Jet [11]

As promising as this concept may seem, one major drawback is that between cores of the tip vortices, a strong downwash is induced. This leads to a reduction in the effective angle of attack of the rear wing and thus a drop in lift. In addition, outside of the cores the upwash causes an increase in effective angle, all of this leads to lift distribution that is far from elliptical and thus reduces the lift to drag ratio of the wing [8]. Whilst this drop in performance is not ideal, it can be offset by increasing the setting angle of the rear wing. Ultimately, the increased aspect ratios of the tandem wing usually lead to superior aerodynamic performance.

However, the vortices pose a greater problem for the aircraft's stability. In pitch the induced angle of attack of the downwash changes as their aircraft pitches up or doing, meaning that the relationship between angle of attack and lift of the rear wing is no longer linear, thus complicating control systems. Additionally, if the vortices incident on each wing are not of equal shape, position, and magnitude then the lift distribution across each wing will be different, resulting in a rolling moment. This could happen in yaw where the horizontal translation causes the vortices to pass over the wings at different points along their spans. The effect is even more pronounced in roll where the rear wing translates horizontally and rotationally. In both cases the additional rolling moment will make the control system more complicated or potentially even result in a positive feedback loop which causes the aircraft to lose control.

Therefore, by being able to accurately model the behaviour of the wake it will be possible to understand these effects which are currently not well documented. It will then also allow engineers to quickly test if an aircraft's stability is significantly affected by the wake of the front wing and assist with control system development.

1.4. Aims & Objectives

After reviewing the salient literature, the VEM was highlighted as being a potential low fidelity replacement to CFD in certain circumstances. As such the objectives listed below are based on the aim of trying to produce, understand and execute a VEM simulation to tandem wing aircraft.

- Develop a model using the VEM to accurately track vorticity bearing points and thus the development of the wake of an airfoil.
- Investigate the effects of different input parameters on model behaviour to ensure the model is efficient and valid, as well as provide a framework for creating a valid VEM model.
- Use the model to correctly represent the velocity field of a 2D cross section downstream of the wing.
- Investigate the effects of the wake of the front wing on the aerodynamic performance of the rear wing and consequently the overall stability of a tandem wing aircraft. Identifying if the effects are a cause for concern and tracking the behaviour through a manoeuvre profile.

1.5. Report Structure

The report is structured in a standard scientific format, with 6 sections including an introduction, literature review, methodology, results, discussion, and conclusion. While the literature review, discussion, and conclusion will follow convention, the methodology and results will be structured specifically for this paper. The methodology section includes a discussion of the aim and reasoning behind the methods used, as well as outlining the computational resources used and the selection of a wing design to act as a base configuration. It also discusses the theory behind the techniques applied and provides a detailed discussion of the work that will be carried out.

Whilst sensitivity studies and model validation are typically included in the methodology section, in this paper they will be included in the results section. This is because the main aim of the project is to demonstrate that the VEM can be used to replicate physical wakes and to show how this can be achieved. Therefore, it is more appropriate to present the sensitivity studies and validation experiments in the results section, where the findings can be discussed in the context of the main results.

Furthermore, the results section will provide specific details about the setup of each experiment in order to make navigation easier and because some studies were conducted ad hoc as new information surfaced.

2. LITERATURE REVIEW

2.1. Aircraft Wake Development

2.1.1. Stages of Wake Development

When assessing the wake of an aircraft, it is essential to differentiate the different stages of its development and the associated changes in properties. These regions are the near, intermediate, and far flow fields. It is important to understand which regions apply to your experiment and design your methodology appropriately; in the case of a tandem wing aircraft the area of concern is several chord lengths downstream of the fore wing.

The near field wake is considered to be the region within one to two chord lengths of the trailing edge [12], where the behaviour is heavily dependent on the geometry and motion of the airfoil. In this region, the formation of smaller secondary vortices is common and in the near field they do not have time to merge with the primary vortex. In addition, they are known to heavily impact the tangential velocity profile of the flow [13]. This is especially true for wings with blunt edges, where the secondary and primary vortices are of a similar magnitude in strength - as shown in Figure 5. Furthermore, flow

in this region is highly unsteady and three dimensional with phenomena such as boundary layer separation adding additional complexity to the flow. These features make it challenging to accurately model the near field wake using simplified techniques such as the VEM. Therefore sophisticated methods such as large eddy simulations [14] or direct numerical simulations are required to model the flow with a high degree of accuracy.

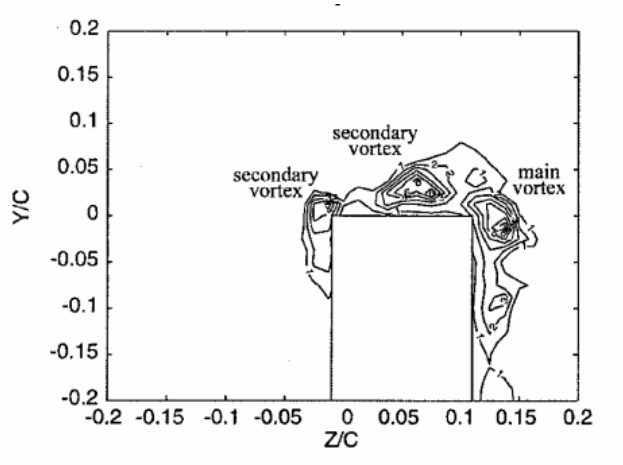

Figure 5 - 2D cross section displaying primary and secondary vortices in near field wake where Z=vertical distance, Y=distance parallel to span, C=chord length of airfoil [15]

Although the categorisation of the far field can vary depending on the specific problem and the context in which it is being studied, it is generally considered to be beyond several chord lengths downstream [12]. It is described as the region where the impact of the atmosphere has become dominant [16], resulting in the decay of the tip vortex, as well as changes in the shape and trajectory of the wake that are not influenced by the initial circulation of the wing. However, the VEM can be used to model the flow by including a numerical dissipation term that accounts for the effects of viscous decay [17]. But this is only valid under ideal conditions and assumes that there are no external influences on the wake, such as wind gusts or interactions with other objects. Therefore, the accuracy of the VEM results in the far field wake can be affected by the choice of the numerical dissipation term and other modelling assumptions, and as such results should be validated using experimental data or other numerical methods.

The intermediate region of the wake lies between the near and far fields and is where the vortex is assumed to have completed its rollup process and is well formed [18]. The behaviour of the flow within this region is heavily dependent on the free stream velocity, angle of attack and shape of the airfoil. If the airfoil is operating in the linear region, such as at low angles of attack then the behaviour of the wake will be simple and dominated by the tip vortices. However, at higher angles of attack the flow is much more complex, with multiple vortices interacting. This leads to a dynamic and constantly changing flow where these vortices merge, breakup and reform. As such the 2D VEM presented can give accurate results so long as the flow remains attached, showing that it is suitable for modelling tandem wing aerodynamics at moderate cruise speeds and low angles of attack.

2.1.2. Areas of Research

The key areas of interest of research into the behaviour of the wake are concerned with formation flight [19], in air refuelling [20] [21], vortex evolution in ground effect [22] and aircraft spacing requirements [16] [23] [24].

The decay of the wake and its effect on aircraft spacing requirements is by far the most studied topic within the literature, with coverage of experimental [23] [25] and computational [26] [27] [28]

methods. It is concerned with better predicting the decay of the wake and looking into methods of increasing the rate of decay to avoid a wake vortex encounter. The reason for this is that by reducing the required spacing between aircraft, the take-off and landing frequency at airports can be increased. Recent developments have been made in understanding the rollup and dynamic instability of vortex pairs, however this work is yet to provide proven and robust methods to categorise and control wake vortices from the near to far field [29]. Additionally, the impact of the atmosphere on wake vortex transport and decay is now largely understood when ambient influences are treated separately, but the full range of possible combinations of environmental factors has not been explored yet. All of this, coupled with the fact research is mainly focused on the effects within the far field, mean that it does not provide too much specific insight into the methods within this paper.

Figure 6 - Passenger Aircraft Wake Rollup [30]

One research area that is highly applicable to this paper is investigations into the interference between tanker wing wake roll-up and the receiver aircraft during refuelling. Firstly, because the receiver aircraft typically refuels in a position of around one span downstream of the tanker [21], it is operating in the intermediate wake region. Additionally, the main area of concern is the stability of the following aircraft, as such it is also looking at the impact of one lifting surface on the performance of another, with the main differences being that the two surfaces are not mechanically coupled like the tandem wing and the vertical separation is often greater. One study utilising the VEM to research the lateral and directional stability during air-to-air refuelling [20] is particularly valuable. Much like what will be done in this paper it estimated that the downwash and sidewash induced by the wake of the tanker and then uses this to estimate the aerodynamic loads on the trailing aircraft by using an appropriate twist corresponding to the local downwash and sidewash angles. This is then used to find the change in the side force, yaw and role derivatives, relative to the vertical displacement between the two aircraft. These results are recorded at a constant lift coefficient and thus angles of attack for both aircraft and as such does not touch upon the dynamic behaviour during manoeuvre. Additionally, their results show to agree qualitatively with flight test observations at similar conditions. Although this is promising, precise experimental data would be needed to accurately assess if the method can accurately predict aerodynamic behaviour rather than simply display similar correlations. It also goes on to show that the tanker fuselage does not need to be represented as experimental results have shown that its impact is negligible. Additionally, the researchers used an arbitrary smoothing factor and timestep, not exploring their effect on results which is known to be significant. Thus, further research is needed to assess how parameters in the discretisation of the aerodynamic equations affect both the accuracy and validity of results.

2.2. Tandem Wing Aircraft

2.2.1. Research Methods

Currently there is a reasonable amount of research data based on tandem wing aircraft, with 1450 articles on Google Scholar matching “tandem wing”. It must be noted that a large amount of these results are interesting flapping tandem wing micro-UAV’s, which is not of concern to this study. However, the majority of modern studies focused on modelling the stability of tandem wing aircraft do so using traditional CFD methods [31] [8] [32] [33] [34], with 467 results for “tandem wing” & “CFD”. Although these studies are highly valuable, the computational resources required to run accurate simulations often limits them to a single aircraft design or a limited number of parametric studies, giving very specific and circumstantial results. Additionally, although CFD can be used to recreate manoeuvres by changing the freestream properties or updating the mesh to capture changes such as aileron movements, it adds a great amount of complexity to the process and does not appear to have been done in literature.

For example, a paper by Figat [26] provides a detailed analysis of the aerodynamic behaviour of a single tandem wing concept. This paper offers moment coefficient results for each airfoil and pressure distribution across the aircraft at a range of angles of attack (AOAs), which cannot be done using the VEM. The study further investigates the effects of flap placement on each wing and evaluates the trim conditions. Consequently, the paper provides a comprehensive insight into the stability characteristics of a tandem wing aircraft that numerical methods cannot provide. Figat found that it is more practical to place control surfaces on the rear wing to reduce the complexity of the aerodynamic coupling. Moreover, the study reveals that using flaps on both wings to achieve trim would be more aerodynamically efficient than using them on one wing, but achieving trim with one set of flaps is more feasible. These findings are significant and offer valuable insights into the design of tandem wing aircraft.

One study by Hao Cheng and Hua Wang [35] uses an adaptation of Prandtl’s lifting line theory alongside a vortex panel method to predict the lift coefficient of a tandem wing configuration. The simplicity of this method allowed the researchers to conduct a large array of experiments in a short timeframe, on top of this the inputs can be easily changed to evaluate additional configurations. Furthermore, the method was shown to produce results for total lift coefficient vs angle of attack that agreed with adjacent CFD and wind tunnel results, within the linear region.

This study gave a comprehensive overview of how design parameters affect the aerodynamic performance of a tandem wing aircraft under static conditions. This included modelling the effect on the lift distribution across each wing when changing parameters such as relative vertical and axial position, angle of attack and span of each wing. It showed that the sectional lift coefficient of the rear wing was only reduced for the span that is directly behind the rear wing or if the front wing has a greater span then the rear wing will display an elliptical lift distribution. Additionally, it was shown that as the distance axial distance between the fore and hind wing (“stagger”) was increased, the sectional lift coefficient increased slightly, due to the strength of the downwash reducing; however, this was only significant up to 3 chord lengths downstream. The vertical displacement between the pair (“gap”) was shown to have an even greater impact on the aerodynamic performance of the hind wing, as shown in Figure 7. One unexpected phenomenon found was that as the angle of attack of the hind wing was increased the lift coefficient of the forewing increased slightly, they say this is because the upwash effect is strengthened to increase the effective angle of attack.

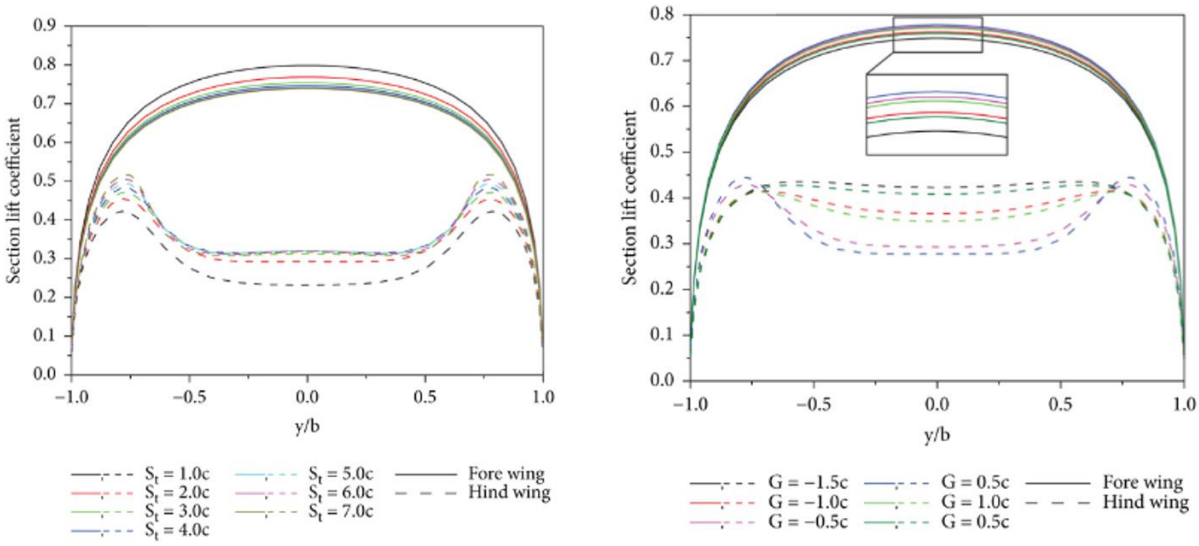

Figure 7a & 7b - Effect of stagger (7a) & gap (7b) on the sectional lift coefficient across the dimensionless span of the Fore & Hind wings

As promising as this method is for quickly evaluating the aerodynamic performance at the early stages of aircraft design, there are some limitations. Firstly, it does not account for time and as such the downwash incident over the hind wing is taken as an instantaneous function of the forewing design. Therefore, the dynamic performance during manoeuvres cannot be assessed as the method does not account for the change in relative position of the rear wing as the movement is performed. Additionally, the method does account for the rollup of the tip vortex and so does not account for the rotational behaviour of the vortices and sidewash, this may lead to a inaccurate lift distribution of the rear wing. However, unlike the 2D vortex element that is to be used in this paper it is transportive, as evidenced by the front wing being influenced by the rear wing.

2.3. Vortex Element Method

One of the greatest advantages of the VEM is that it is highly adaptable and as such it has been widely applied in a range of fluid dynamics problems. This includes a variety of problems such as the flow over airfoils [36], the simulation of the flow around bluff bodies, such as circular cylinders [37] and the flow around wings with complex shapes [38]. However, this study is concerned with utilising the method for modelling the dynamics of the vortex sheet for which there are several variations that can be used. Two of the most commonly used variations are the vortex lattice method (VLM) and discrete vortex methods (DVM).

Although the VLM is an efficient method for analysing overall aerodynamic characteristics of aircraft, its assumption of a flat wake limits its ability to model flows with strong vortex interactions or when the tip vortex dominates the wake structure [39]. Moreover, the VLM cannot display the rollup, which is crucial for analysing the strength and behaviour of the vortex.

DVM are a useful tool for modelling the flow field around aircraft due to their ability to capture the complex, non-linear behaviour of vortices. Unlike the VLM, DVMs do not assume a flat wake and can accurately predict the behaviour of tip vortices, including the rollup. Additionally DVMs are suitable for prediction of the aircraft vortex wake at every stage of its evolution [40]. As such DVMs are well suited for modelling flows with strong vortex interactions or complex wake structures, such as those found in close formation flight [19] or ground effect [22], with the referenced papers showing the methods ability to accurately model rollup. While DVMs are generally more computationally

expensive than VLMs, their ability to account for the tip vortex rollup make them better suited to the requirements of this paper.

The exact method that will be used in this study is the same as the one used by Cho [22] and Han [19] referenced in the previous paragraph. It was developed by Robert Krasny in his paper "Computation of vortex sheet roll-up in the Trefftz plane" [41]. In this paper the shed vorticity within the wake is represented by a vortex sheet and the spatial coordinate in the direction of the free stream is replaced by a time coordinate. As such the problem is transformed from a steady three spatial dimension free boundary problem to an initial value problem for the vortex sheets evolution as a curve in 2D space, known as the Trefftz plane. The initial vorticity enters the wake by specifying the spanwise circulation distribution, which is determined using classical lifting line theory. This reduces the complexity of the problem and makes it far simpler to model. However, by making it an initial value problem the effect of atmospheric conditions on the wake cannot be accounted for, however this is not an issue in the intermediate region of the wake as behaviour is overwhelmingly influenced by the shape and behaviour of the airfoil. Additionally, by working in the Trefftz plane the method is not transmissive and so 3D flow effects cannot be accounted for, which may cause inaccuracy if initial conditions change over time or if the freestream velocity is not constant.

3. METHODOLOGY

3.1. Selection of Baseline Configuration for Tandem Wing Experiment

To properly investigate the effects of various parameters on the aerodynamics of tandem wings, a baseline configuration is set for the experiment. This baseline configuration provides a reference point from which different parameters can be varied and their effects observed. This is critical, as it enables a proper comparison and interpretation of the data obtained. By having a consistent starting point it is ensured that any differences observed in the experimental results can be attributed to the variation in parameters being tested, rather than to differences between experiments. Furthermore, selecting a baseline design from literature ensures that the design is both feasible and relevant to real-world applications. This is important in ensuring that the results obtained from the experiments are applicable and useful for future design applications.

As such the selected wing design aims to ensure that it operates within appropriate bounds of the VEM, rather than creating a stable or efficient aircraft. For this purpose, mirroring eVTOL concepts such as the Lilium Jet is ideal as they operate at a cruise speed of 83m/s [42]. Working at a Reynolds numbers where the linear region of the selected airfoil extends over a wide range, whilst ensuring that compressibility effects are not a concern. These concepts operate firmly in the intermediate wake region, with axial wing separations of 4-8 chord lengths. Furthermore, to agree with good tandem wing design principles, vertical separation of the two wings will be 1.5 chord lengths of the front wing. This choice also helps with the sensitivity studies as a low vertical separation would cause the vortex core to pass over the rear wing, resulting in exaggerated effects from small changes in position or behaviour. Additionally, although many concepts including the Airbus Vahana air taxi utilise wings of the same span, to study the effects of upwash a slightly smaller front wing will be used. Finally, although it is hard to find data on exact dimensions for any tandem wing aircraft the estimated dimensions of the Lilium jet are shown in Table 1.

Table 1 - Lilium Jet Dimensions [43]

Rear Wing Dimensions	**Wingspan (**m)	**6**
	Root Chord (***m***)	0.78
	Tip Chord (***m***)	0.42
Front Wing Dimensions	Wingspan (***m***)	2.6
	Root Chord (***m***)	0.56
	Tip Chord (***m***)	0.48
General Parameters	Gap (***m***)	2
	Stagger (***m***)	0.3

The selected configuration is outlined in Table 2. Although based on the Lilium, the size of the front wing was increased to add more vorticity to the flow, the gap was then increased proportionally to the increase in chord length as well. Then the gap was set to be 1.5 chord lengths and the freestream velocity was rounded to 80ms^{-1}.

Table 2 - Base Configuration Dimensions

Rear Wing Dimensions	**Wingspan (**m)	**6**
	Root Chord (***m***)	0.9
	Tip Chord (***m***)	0.6
	Area (m^2)	4.5
	Aspect Ratio	8
Front Wing Dimensions	Wingspan (***m***)	4
	Root Chord (***m***)	0.6
	Tip Chord (***m***)	0.4
	Area (***m*^{2}**)	2
	Aspect Ratio	8
General Parameters	Stagger (***m***)	3
	Gap (***m***)	0.75
	Freestream Velocity (***ms*$^{-1}$**)	80

3.2. Computational Methods

After thoroughly considering the project requirements and the available programming languages, MATLAB was chosen as the most appropriate for this study. One of the main reasons for this is its ability to work with matrices. The VEM relies heavily on matrix operations and so MATLAB's inbuilt matrix functionality it an ideal choice for this project. In addition, MATLAB has a wide range of graphical options, making it easier to visualise the results and analyse the data.

While other programming languages such as Python and C++ can also handle matrix manipulation, MATLAB's syntax is designed specifically for matrix operations, making it more efficient and easier to use. Furthermore, I personally have extensive experience using MATLAB and given the limited timeframe of the project, the added constraint of learning a new language would have resulted in a tighter project deadline. Therefore, based on its matrix handling capabilities, graphical options, ease of use, and my personal experience, MATLAB was chosen for this study.

3.3. Theory

3.3.1. Circulation Distribution

3.3.1.1. Classical Lifting Line Theory – Fore Wing

Developed by Prandtl between 1911 and 1918, lifting line theory is a theoretical framework used to analyse the aerodynamics of finite wings. The utility of the method is so great that it is still in use today for the preliminary calculations of finite wing characteristics [12], due to it being simple, computationally efficient, accurate and flexible. While classical lifting line theory is a widely used method, certain criteria must be met to ensure its accuracy. Firstly, it is limited to low subsonic Mach numbers as it cannot account for compressibility. Additionally, it assumes an infinitely thin wing and neglects the effects of viscosity, turbulence, and surface roughness. Consequently, the classical lifting line theory does not consider stall phenomenon and assumes that the wing operates with fully attached flow within the linear region. However, for the conditions present within this study these assumptions are reasonable.

This method works by replacing a finite wing with a lifting line along which the circulation varies continuously. For a general lift distribution the circulation distribution can be approximated as the Fourier sine series shown in Equation 1.

$$\Gamma(\theta) = 2bV_\infty \sum_{1}^{n} A_n \sin(n\theta) \tag{1}$$

Where θ represents the spanwise position according to the transform shown in Equation 2.

$$y = -\frac{b}{2}\cos(\theta) \tag{2}$$

To find the Fourier constants (A_n) Equation 3 must be solved as a set of simultaneous equations by taking regular intervals across the span for $-\frac{b}{2} < y < 0$. For all simulations ran in this study 50 Fourier coefficients were used as above this number the accuracy of the solution does not increase. Additionally, because finding the circulation made up such a small percentage of the computational processes of each simulation the additional efficiency of reducing the number added no benefit to the run time.

$$\alpha(\theta) - \alpha_{L=0}(\theta) = \frac{2b}{\pi c(\theta)} \sum_{1}^{n} A_n \sin(n\theta) + \sum_{1}^{n} nA_n \frac{\sin(n\theta)}{\sin(\theta)} \tag{3}$$

It must be noted that for the forewing there is no geometric or aerodynamic twist, so $\alpha(\theta)$ & $\alpha_{L=0}(\theta)$ are constants and $c(\theta)$ varies across the span depending on the taper ratio. From this the circulation distribution, sectional lift distribution, sectional lift coefficient and total lift coefficient can be found according to Equations 4, 5 and 6 respectively.

$$L'(\theta) = \frac{2\Gamma(\theta)c(\theta)}{V_\infty} \tag{4}$$

$$C_l(\theta) = \frac{2\Gamma(\theta)}{V_\infty} \tag{5}$$

$$C_L = \frac{b^2}{S}\pi A_1 \tag{6}$$

3.3.1.2. Adapted Lifting Line Theory for a Twisted Wing – Hind Wing

The vertical component of the forewing wake causes a change in the local effective angle of the hind wing, this effect is equivalent to changing the geometric twist across the span. In this case classical lifting line theory is no longer valid as the changing operating conditions result in a change in the Fourier coefficients along the span. As such the following adapted lifting line theory was developed by Phillips [44] to evaluate the circulation distribution for twisted wings. The solution is obtained by using the change of variables shown in Equation 7.

$$\alpha(\theta) - \alpha_{L0} \equiv (\alpha - \alpha_{L0})_{root} - \Omega\omega(\theta) \tag{7}$$

Where Ω is evaluated at a reference position such that

$$\Omega \equiv (\alpha - \alpha_{L0})_{root} - (\alpha - \alpha_{L0})_{ref} \tag{8}$$

$\omega(\theta)$ is then defined as the twist distribution normalised with respect to the twist at the reference point as shown in Equation 9

$$\omega(\theta) \equiv \frac{\big(\alpha(\theta) - \alpha_{L0}(\theta)\big) - (\alpha - \alpha_{L0})_{root}}{(\alpha - \alpha_{L0})_{ref} - (\alpha - \alpha_{L0})_{root}} \tag{9}$$

This normalised twist distribution function is independent of angle of attack and by taking the reference point as the point of maximum twist (in this instance downwash) it varies between 0 and 1. This is then substituted into Equation 3 to give the following relationship.

$$(\alpha - \alpha_{L0})_{root} - \Omega\omega(\theta) = \frac{2b}{\pi c(\theta)}\sum_1^n A_n \sin(n\theta) + \sum_1^n nA_n \frac{\sin(n\theta)}{\sin(\theta)} \tag{10}$$

The Fourier coefficient A_n in Equation 10 is then written as

$$A_n \equiv a_n(\alpha - \alpha_{L0})_{root} - b_n\Omega \tag{11}$$

Where the Fourier coefficients a_n and b_n are obtained as follows.

$$\sum_1^n a_n \left[\frac{4b}{\tilde{C}_{L,\alpha}c(\theta)} + \frac{n}{\sin(\theta)}\right]\sin(n\theta) = 1 \tag{12}$$

And

$$\sum_{1}^{n} b_n \left[\frac{4b}{\tilde{C}_{L,\alpha} c(\theta)} + \frac{n}{\sin(\theta)} \right] \sin(n\theta) = \omega(\theta) \tag{13}$$

These are then solved as a set of simultaneous equations and then substituted into Equation 11 to find A_n, which is subsequently used in the same manner as in classical lifting line theory.

3.3.2. Wake Evolution

In order to model the roll up of the wake the methodology outlined by Krasny [41] is followed, with key equations highlighted below.

The vortex sheet is defined as the curve $z(\Gamma, t) = x(\Gamma, t) + iy(\Gamma, t)$ and the evolution equation is defined in Equation 14, noting that the spanwise position is transformed such that $\cos(\alpha) = 2y/b$.

$$\frac{\partial \bar{z}}{\partial t} = \int_0^{\pi} K(z - \tilde{z}) \Gamma'(\tilde{\alpha}) d\tilde{\alpha} \tag{14}$$

Where $K(z)$ is the Cauchy kernel

$$K(z) = -\frac{1}{2\pi i z} \tag{15}$$

However, this becomes singular when a vortex filament intersects with itself or another filament, leading to numerical instability and inaccurate results. To address this issue Krasny introduced a smoothing factor (δ) into the Cauchy kernel, which is a positive constant that acts to control the width of the smoothing function used to regularise the kernel. By using a smoothed kernel, the velocity field becomes continuous and differentiable everywhere, avoiding the numerical instability and inaccuracy associated with the singularities of the unsmoothed kernel. Additionally, Krasny then states that the solution of the δ equation (Eq 16) converges to the solution of the vortex sheet equation (Eq 14), where the δ equation is defined as follows.

$$\frac{\partial \bar{z}}{\partial t} = \int_0^{\pi} K_\delta(z - \tilde{z}) \Gamma'(\tilde{\alpha}) d\tilde{\alpha} \tag{16}$$

And $K_\delta(z)$ is the smoothed kernel.

$$K_\delta(z) = K(z) \frac{|z|^2}{|z|^2 + \delta^2} \tag{17}$$

This can then be solved numerically by discretising the equation. First the vortex sheet it approximated as $z_j(t) = x_j(t) + iy_j(t)$ at equidistant α along the span. The integral in Equation 16 is then approximated using the trapezoidal rule, resulting in a set of ordinary differential equations for the motion of the points as shown.

$$\frac{d\bar{z}}{dt} = \sum_{k=1}^{2N+1} K_\delta(z_j - z_k) w_k \tag{18}$$

Noting that $k = j$ is omitted from the sum and the quadrature weights (w_k) are defined as

$$w_k = \frac{\Gamma'(\alpha_k)\pi}{2N} \tag{19}$$

The Runge-Kutta 4th order method (RK4) was chosen over the Euler method for the time integration of the Equation, primarily due to its higher accuracy and stability [45]. The RK4 method uses four function evaluations per time step, leading to more accurate numerical solutions, which is particularly advantageous for simulating complex flows where small errors can accumulate over time. Additionally, the RK4 method is more stable than Euler, making it more suitable for simulating flows with strong vorticity. However, the main disadvantage of RK4 is its higher computational cost due to the four function evaluations per time step, which was deemed justified in this study given the additional stability achieved.

Although tracking the wake rollup gives valuable insight into the behaviour of the wake, to validate against experimental results and assess the impact of the wake on objects downstream the velocity of the flow must be found. This can be done by discretising the space you wish to evaluate into "particles" located in a 1D or 2D cross section of the flow, with each particle being assigned a position in the complex plane, $z = x + iy$. Then the instantaneous velocity of each point can be found by using Equation 18 in the same manner as calculating the roll up of the vorticity, however z_j represents the particles whose velocity you are trying to find and z_k represents the vorticity bearing points. When working on finding these velocities the smoothing factor used will be referred to as the rear wing smoothing factor or SF2.

3.4. Workplan

3.4.1. Validation of LLT and VEM Code

Lifting line theory is accepted as an accurate method and the reliability of the VEM in tracking vorticity has also been demonstrated. However, because this study involves the development of new code and so it is crucial to ensure its accuracy and absence of errors.

Classical lifting line theory is a well-established and simple method for calculating spanwise loading on wings, and therefore, it will not be evaluated in this study. However, because modifications for a twisted wing are more nuanced, they will be checked. Since relevant experimental results for a twisted wing could not be found, a comparison was made against the computational results from paper that provided the method (see Figure 8), ensuring at least that the code is correct.

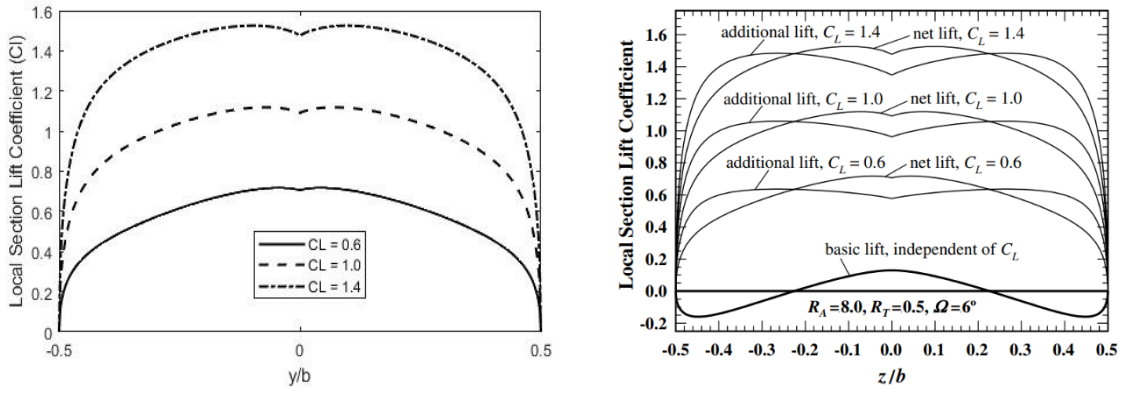

Figure 8(a) & 8(b) - Sectional Lift Coefficient for Twisted Wing for Comparing My Code (A) to Example Study (B)

Additionally, the correctness of the VEM code was established by replicating Krasny's experiments that utilise an arbitrary elliptical lift distribution (see Figure 9).

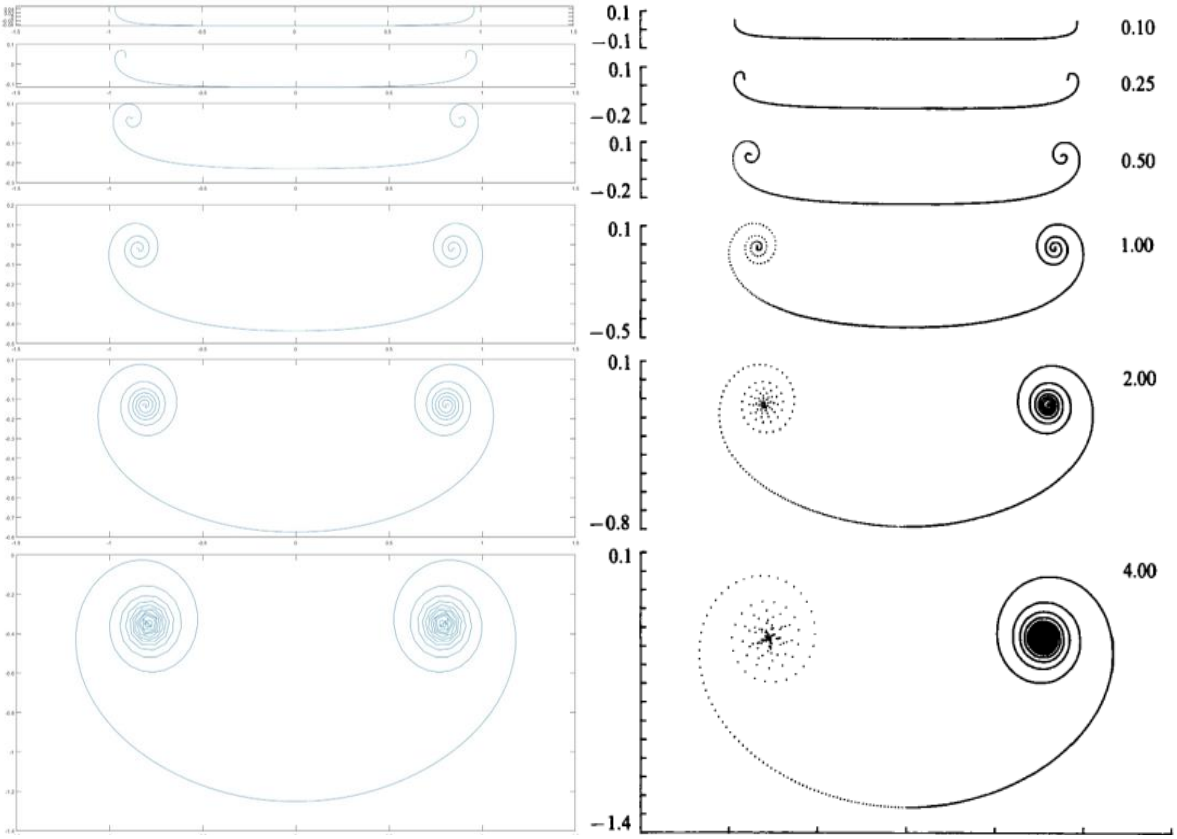

Figure 9(a) & 9(B) - Wake Rollup for Comparing My Code (A) to Example Study (B)

By conducting these validation exercises, any limitations of the theory or numerical methods can be identified, and any observations made in the later stages of the study will be attributed to these constraints.

3.4.2. Sensitivity Analysis of Discretisation Parameters

When solving such problems numerically, it is important to understand the effect of changing parameters used to discretise the problem. In the case of VEM, these parameters include the timestep, number of vorticity bearing points in the VEM and the smoothing factor for the wake rollup and velocity determination. Evaluating the resolution of the spatial and time steps is crucial, as if it is too low, the results will be invalid, and if it is too high, the code will not be computationally efficient, and simulations will take an excessive amount of time to run. Therefore, sensitivity studies will be carried out on these variables to ensure they are optimised.

The aim of these studies is not to ensure the results are perfectly recreating flow conditions, but instead to find where behaviour is independent of the resolution of these variables. To achieve this, a test case of finding the total lift coefficient of the rear wing will be evaluated for the time step and vorticity points, as it is a function of the location of the vortex core, distribution of vortex points along the lifting line, shape of the rollup, and stability of the roll-up, all of which are highly important.

The smoothing factor is a bit more complex, as the behaviour induced by adjusting it is also heavily influenced by other factors, especially the number of vortex points. As such, the effect will be quantitatively and qualitatively evaluated. If the smoothing factor is too high, the vortex sheet will not roll up sufficiently, and if it is too low, the core of the vortex will become unstable. Additionally, Krasny [41] found that so long as the vortex remained stable, decreasing the smoothing factor increases the

number of turns in the vortex, which in turn increases its accuracy. Therefore, the minimum smoothing factor at which the vortex remains stable needs to be found. Overall, these sensitivity studies are crucial to ensure that the parameters used to discretise the problem are optimised for accurate and efficient simulations using VEM.

3.4.3. Replicating Physical Flow Properties

Once the models are shown to work correctly and the discretisation of the problem is fully understood, it is then possible to explore the key aim of whether or not the VEM can be used to accurately replicate physical flow behaviour. The key features of the flow are the location of the core of the tip vortex and the additional velocity induced by the vorticity. In this case the location of the vortex core at each tip is defined as position of z_1 and z_{2N+1} of the vorticity bearing points and the induced velocity can be divided into the vertical and spanwise components V_X and V_Y respectively.

To validate the numerical method used in this study, it would ideally be compared to experimental data through a comparison of the velocity field of a two-dimensional cross section of the wake. This type of comparison is useful as it allows for a detailed comparison of the flow field in different regions and provides insight into the accuracy of the numerical model across them. But, despite extensive efforts, suitable experimental data for this comparison could not be found. This is likely due to the significant amount of effort required to obtain such measurements and the limited need for such results. However, two studies assessing the velocity distribution across a 1D plane in the spanwise direction were found which provide a highly useful comparison still.

The first paper to be used as a test case was McAlister's “NACA 0015 Wing Pressure and Trailing Vortex Measurements” [46]. The wing configurations studied were rectangular and had a constant and untwisted NACA 0015 profile along the span. The experiment was conducted in the NASA Ames 7 by 10-foot subsonic wind tunnel, noting that the walls were placed 1 chord length from the root and 1.9 chord lengths from the tip. At this scale, the wing-tip vortices can interact with the wind tunnel walls, which could lead to differences in the vortex strength and position compared to what would be observed in a free-flight condition. As such comparisons made with the VEM which assumes no flow confinement should be focussed on replicating behaviour and not replicating exactly. Furthermore, the wind tunnel walls can cause blockage effects, which can alter the velocity field around the wing and the resulting vortex. However, the effects of blockage are expected to be small, but it is still important to compare the spanwise loading of the experiment and the simulation to identify the impact of this. Additionally, velocity profiles were measured at various points behind the wing using a two-component laser velocimeter, which is non-invasive and does not affect the flow. Finally, these measurements were taken at a vertical displacement level with the vortex core and the coordinate system is referenced as the origin being centred at the vortex core.

The experiment evaluates the effect of chord, aspect ratio, angle of attack, and wingtip shape as design variables, and investigates their effect on velocity profile, vortex core radius, spanwise displacement of the vortex core, and vertical displacement of the vortex core. This allows for an evaluation of the VEMs sensitivity to a large array of parameters that are crucial in aerodynamic design and identify any shortcomings.

An additional study was found to further validate the VEM for a different airfoil. This study focused on the commonly used NACA 0012 airfoil [47], which is designed for low-speed applications. Like the previous experiment, this study was also conducted in a wind tunnel and suffered from the same issues related to the confined flow. However, this study had some unique features. The free stream velocity used in this experiment was 8m/s, which resulted in a Reynolds number an order of magnitude lower than that of the NACA 0015 airfoil experiment. This characteristic of the airfoil led to a separation of the flow at a lower angle of attack, limiting the range of useful results. Unfortunately,

this experiment provided limited data compared to the NACA 0015 airfoil experiment, with the only useful data being the velocity profile at one position in the intermediate region at an angle of attack of ten degrees. Despite these limitations, the study provided value by validating the VEM for a different airfoil and demonstrating its versatility for multiple experiments with different airfoils.

Also, this study used a different experimental procedure. Hot wire probes were used to measure the flow velocity of the wake and the vortex tracking method to locate the vortex centre. However, the intrusive nature of the probes can potentially alter the flow and cause inaccuracies in the results. To minimise this effect, the probes were carefully positioned and calibrated. Additionally, the velocity profiles obtained from the probes are not continuous functions, however a high resolution was used to mitigate the effect of this.

3.4.4. Tandem Wing Investigation

As highlighted in the literature review, the VEM could be a valuable tool to investigate the dynamic stability of a tandem wing aircraft. So, in order to prove that it is possible to implement a dynamic VEM model and assess the stability of a tandem wing aircraft a simple experiment looking at an aircraft in pitch will be conducted. This will involve pitching the aircraft nose up and comparing a dynamic and static case. In the dynamic case wings will have a vertical velocity relative to the pitch rate which will impact their effective angle of attack and position relative to each other. Whereas the static case will take readings at the same angles of attack but with no pitching action. This test will evaluate the base configuration with the rear wing set at an angle of attack 2 degrees greater than the front wing, to give results that indicate real world tandem wing behaviour.

To simplify the investigation, the aircraft will be modelled although an external force is rotating it about the midpoint of the two wings, rather than the lift over each wing causing a pitching moment about the centre of mass. Although this does not recreate the dynamic behaviour of an aircraft in flight, it still allows the effects of pitch rate and angle on the rear wing behaviour to be seen. Therefore, for the dynamic case the effective angle of fore and hind wing were calculated using Equations 20 and 21 respectively.

$$\alpha_{forewing} = \dot{\theta}t - \tan\left(\frac{\dot{\theta} * stagger}{2V_{\infty}}\right) + \alpha_{set} \tag{20}$$

$$\alpha_{hindwing} = \dot{\theta}t - \tan\left(V_{y-induced} - \frac{\dot{\theta} * stagger}{2V_{\infty}}\right) + \alpha_{set} \tag{21}$$

4. RESULTS

The results displayed in the following section were obtained using the LLT_1, LLT_2_twist & Krasny MATLAB scripts listed in the appendices. However, it must be noted that for each experiment the scripts were modified slightly to fit the requirements of each.

4.1. Analysis of Discretisation Parameters

The first step towards analysing the VEM was to understand how to run the code efficiently and accurately. Hence why sensitivity studies have been carried out on the discretisation parameters. It is important to note that all of these variables are interlinked in a complex fashion and so although the results of the following section give insight into the order of magnitude of which the variables should be selected for further work, care must be taken to ensure that the circumstances of each subsequent experiment is considered and the stability of the vortex is checked. Additionally, all the studies results shown utilise the wing configuration specified previously.

4.1.1. Spatial Resolution of Vorticity Bearing Points

The first variable to be analysed was the number of vorticity bearing points used to model the rollup of the wake. The reason this was selected first was that the number of operations required within the code for the number of spatial points is proportional to its square, whereas it is linearly proportional to other variables. This can be seen in Equation 14 where this variable dictates the resolution of both z_k and z_j. Therefore, by knowing the number of spatial steps to use in subsequent studies, their efficiency can be improved drastically. The variables shown in Table 3 were selected for the test resulting in Figure 10 and they were chosen to be similar to those used by Krasny in his works to give a reasonable starting point.

Table 3 - Discretisation Parameters for Spatial Study

Parameter	Value	Unit
Timestep	0.001	Seconds
Smoothing Factor – Front Wing	0.05	N/A
Smoothing Factor – Rear Wing	0.05	N/A

As seen by the extremely low range of the y-axis in Figure 10 the spatial resolution showed to not affect the stability of the roll up or its motion until very low resolutions; 25 steps gave a CL of 0.1484 but was not included as it ruined the scale of the figure. Additionally, I believe that the small changes observed in Figure 10 can be attributed to the lower resolution of the data, resulting in a more jagged line rather than a smooth curve. It must be noted that the position of the rear wing is situated a suitable distance from the core and so a greater variance may be seen if the proximity is closer or if the core passes over the wing but at least for the further sensitivity studies this is not of concern. As such 400 points were used in future as this gave a fast runtime whilst giving a total lift coefficient that only varied from that at 1200 by 0.0067%.

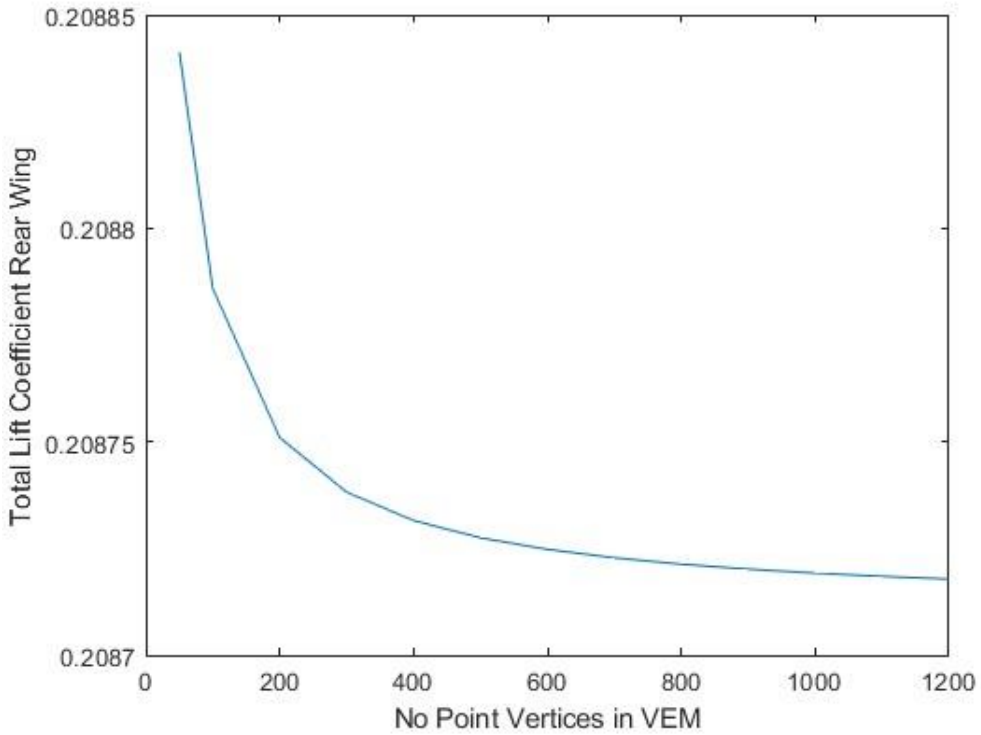

Figure 10 - FIGURE 9 - EFFECT OF Number of Point Vertices On Rear Wing Total Lift Coefficient for Base Configuration

The results depicted in Figure 11 reveal that the difference between 100 and 1200 spatial steps is negligible, except on a micro level, whereas the instability resulting from 25 steps is evident. Hence, it can be deduced that the number of spatial steps does not significantly influence the outcome of the simulation. Nevertheless, it is essential to bear in mind that the base configuration under investigation is subject to incomplete rollup of the vortex, despite having initiated the process. Consequently, with a greater number of turns, the spatial step may have a more pronounced effect, as a higher resolution is necessary to capture the additional turns.

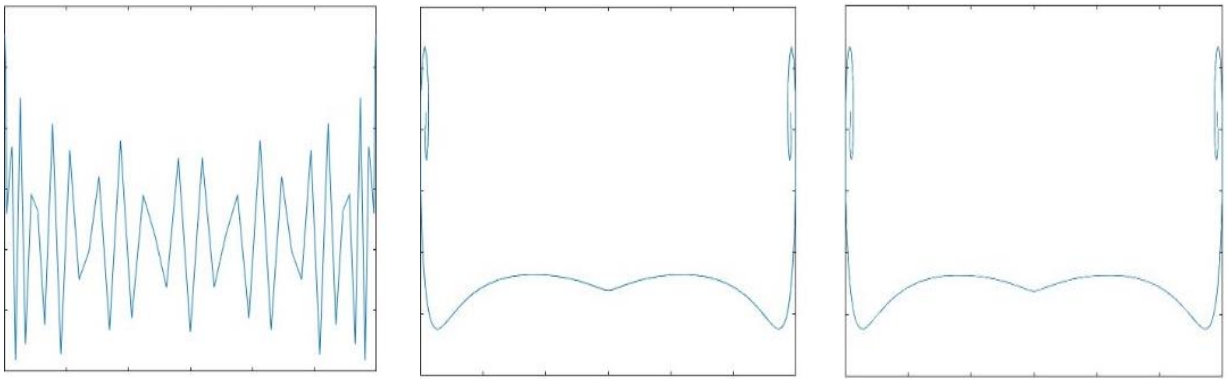

Figure 11a 11b & 11c - Vortex Rollup Shape for 25(a) 100(b) & 1200(c) Point Vertices

4.1.2. Timestep Analysis

Next, the effect of timestep on the stability and validity of the results was evaluated. It is important to note that although there is a linear relationship between timestep and the number of operations, a change of multiple orders of magnitude may be required to obtain stable results. As such, the timestep was considered over the range $\Delta t = 10^{\frac{-i-3}{4}} \; for \; i = 1:1:19$. Additionally, the values of additional parameters used in this simulation are given in Table 4.

Table 4 - Discretisation Parameters for Timestep Study

Parameter	Value	Unit
No Spatial Steps	400	N/A
Smoothing Factor – Front Wing	0.05	N/A
Smoothing Factor – Rear Wing	0.05	N/A

The effect of the timestep on the accuracy and stability of the simulation was investigated for the baseline configuration, with results shown in Figure 12. This shows a convergence at a timestep of around 0.005-0.01, with no significant increase in accuracy at values below this. However, it was observed that above this value, the accuracy decreases. Nevertheless, in the range investigated, it did not appear to become unstable. Despite these results, to ensure the highest level of accuracy and to prevent any potential instability issues, a conservative timestep of 0.001 will be employed in future simulations.

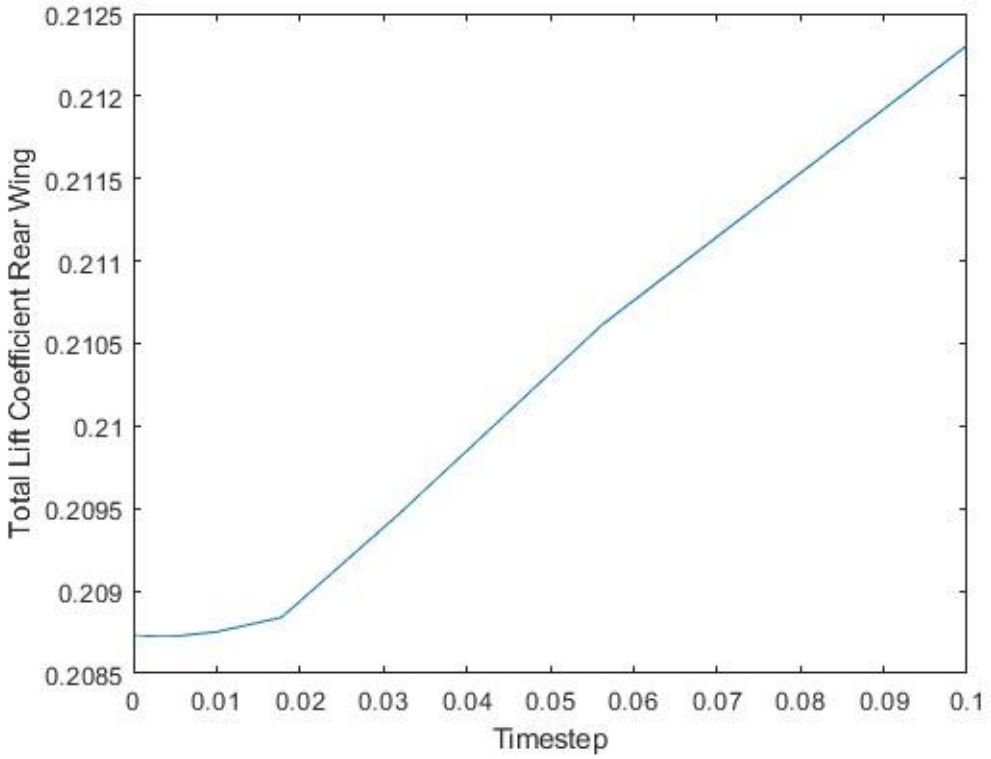

Figure 12 - Effect of Time Step on Rear Wing Total Lift Coefficient for Base Configuration

Although the results in Figure 12 suggest that the convergence of the timestep is a simple process, it was important to see if this was a universal case. As such the experiment was repeated with the front and rear wing dimensions switched. This has the effect of changing the strength of the vortex, the distance downstream relative to the chord of the front wing and the position of the rear wing relative to the core. The results in figure 13 show a drastic change in behaviour, first the convergence happens at around 0.001 which is an order of magnitude lower. Additionally, the solution begins to oscillate in an increasing amplitude as the resolution is reduced, hinting at an unstable solution. This shows the complexity of the issue at hand and as such it is important to check the stability of the vortex for each run unless a considerably conservative resolution is used.

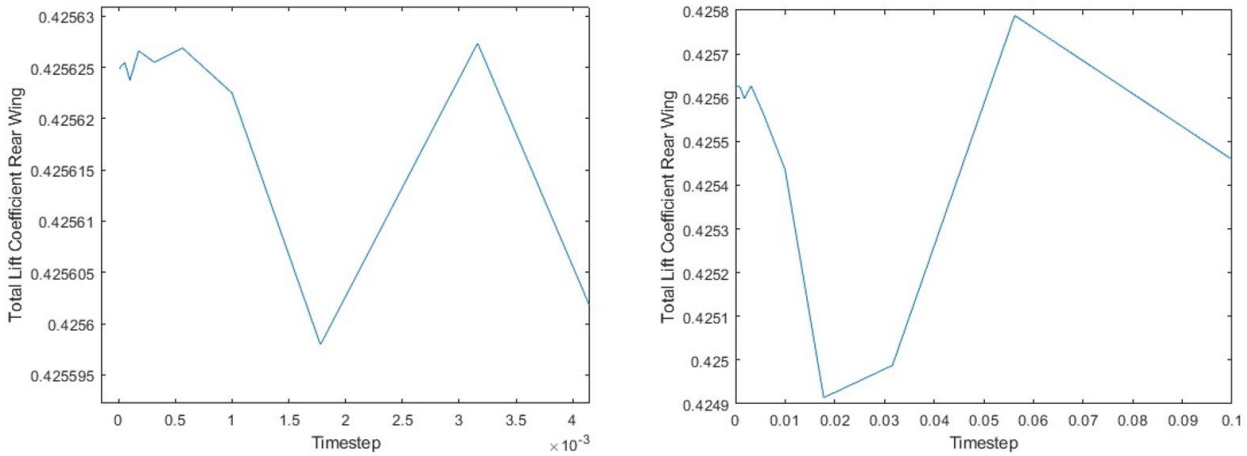

Figure 13(a) 13(b) - Effect of Time Step on Rear Wing Total Lift Coefficient for Larger Forewing from ranges 0-0.004 (A) and 0-0.1 (B)

In the context of numerical modelling, the time resolution is commonly referred to as Δt or the number of timesteps. Both factors are critical in achieving accurate and stable results and although they represent the same thing they can be thought of slightly differently. Δt is related to the physics of the model and can produce instability if set too high. For instance, this can happen in high-velocity situations or large wing planforms where the forces and distances involved are more significant. The effect of this can be seen in Figure 14 where $\Delta t = 0.1$, where each particle travels large distances over each timestep, and its velocity does not adjust and so it overshoots its position at each point resulting in major instability. On the other hand, the number of timesteps is related to the discretization of the model, and if there aren't enough timesteps, the model may not be able to develop accurately. This aspect is more important in situations where the downstream wing is in close proximity or at high freestream velocities where the total time is limited.

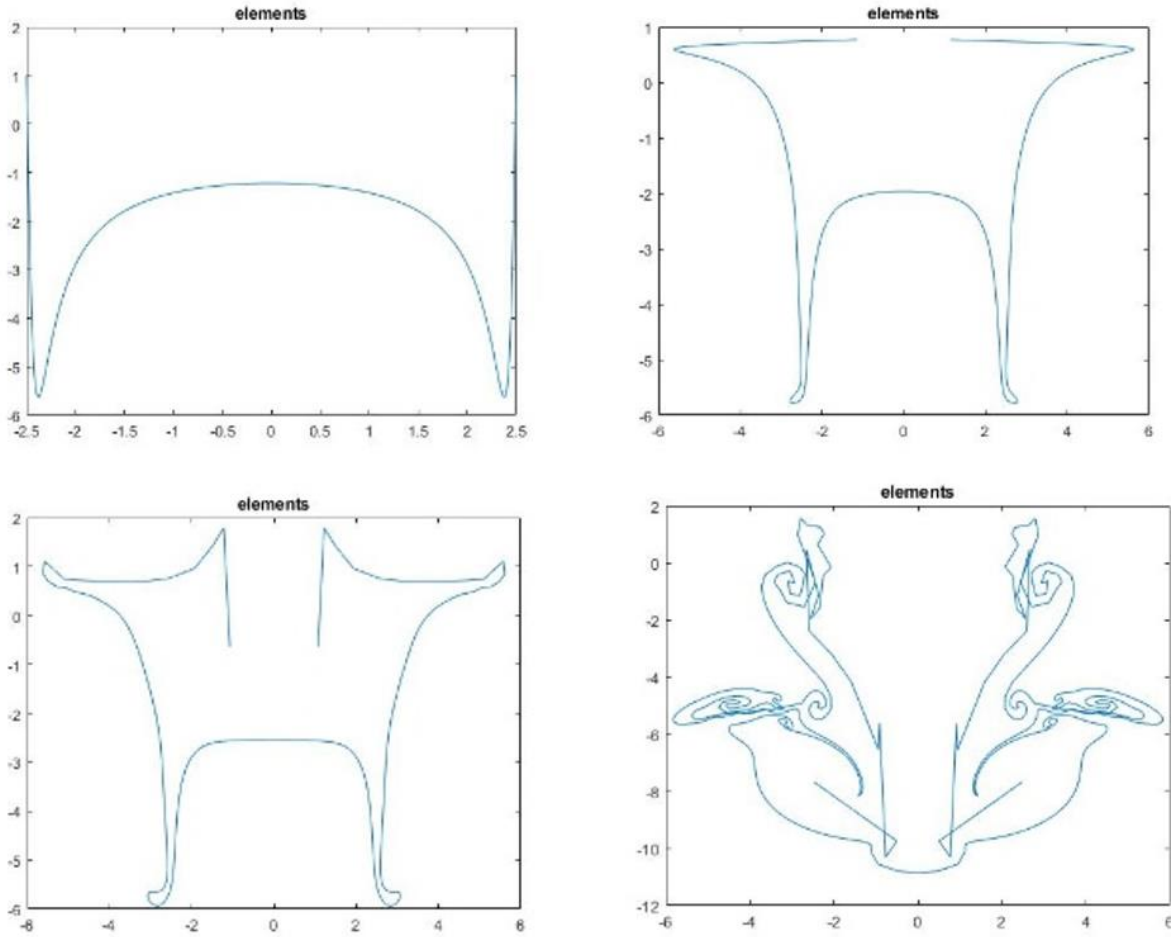

Figure 14(a), 14(b), 14(c) & 14(d) - Unsteady Wake Rollup for Timestep of 0.1 After Time 0.1(a) 0.2(b) 0.3(c) & 1(d) Seconds

4.1.3. Smoothing Factor Analysis – Front Wing

Table 5 - DISCRETISATION PARAMETERS FOR SF1 Study

Parameter	Value	Unit
Timestep	0.001	Seconds
No Spatial Steps	400	N/A
Smoothing Factor – Rear Wing	0.05	N/A

In this test, the impact of the smoothing factor for the wake rollup (SF2) is examined. The results presented in Figure 15, demonstrate that the total lift coefficient diverges as the smoothing factor tends tends to infinity. Whereas below values of 0.025 the solution becomes unstable. This behaviour is expected as this shows the smoothing factor becoming too low for the given time and spatial to provide a stable solution. This can be seen in Figures 16A and B, where the vortex of the core can be seen to become unstable. The opposite effect is seen in Figure 16D, where the excessively high smoothing factor inhibits the rollup of the tip vortex.

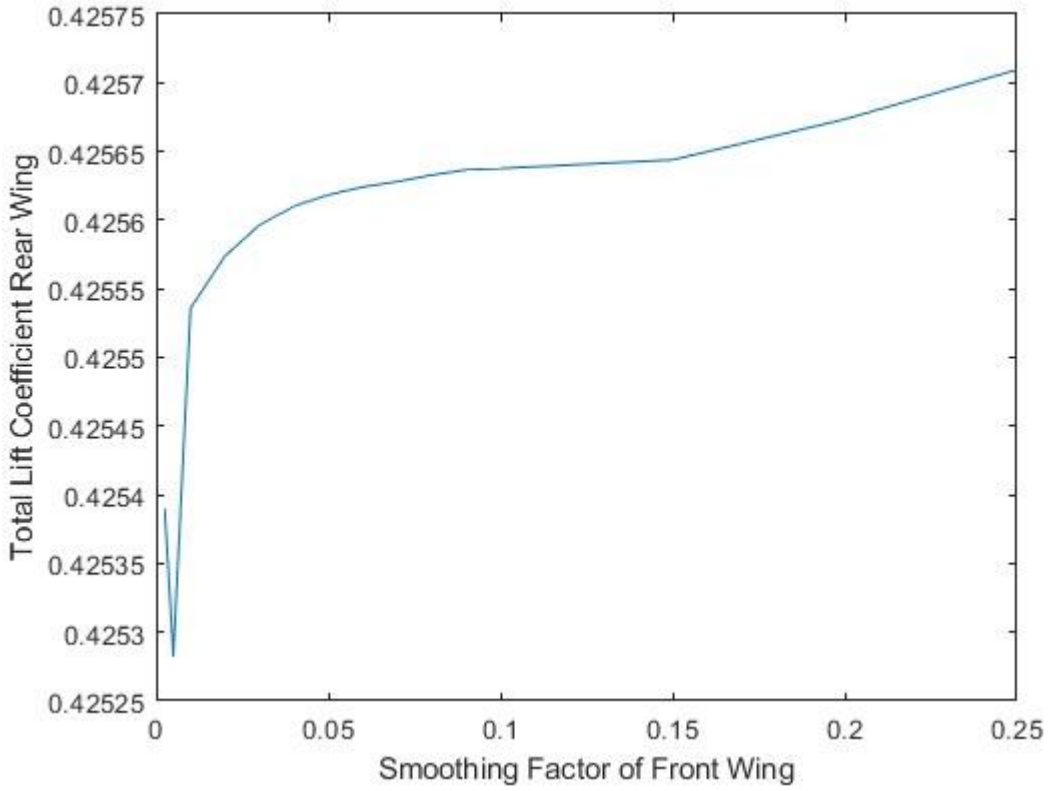

Figure 15 - Effect of SF2 on Rear Wing Total Lift Coefficient for Base Configuration

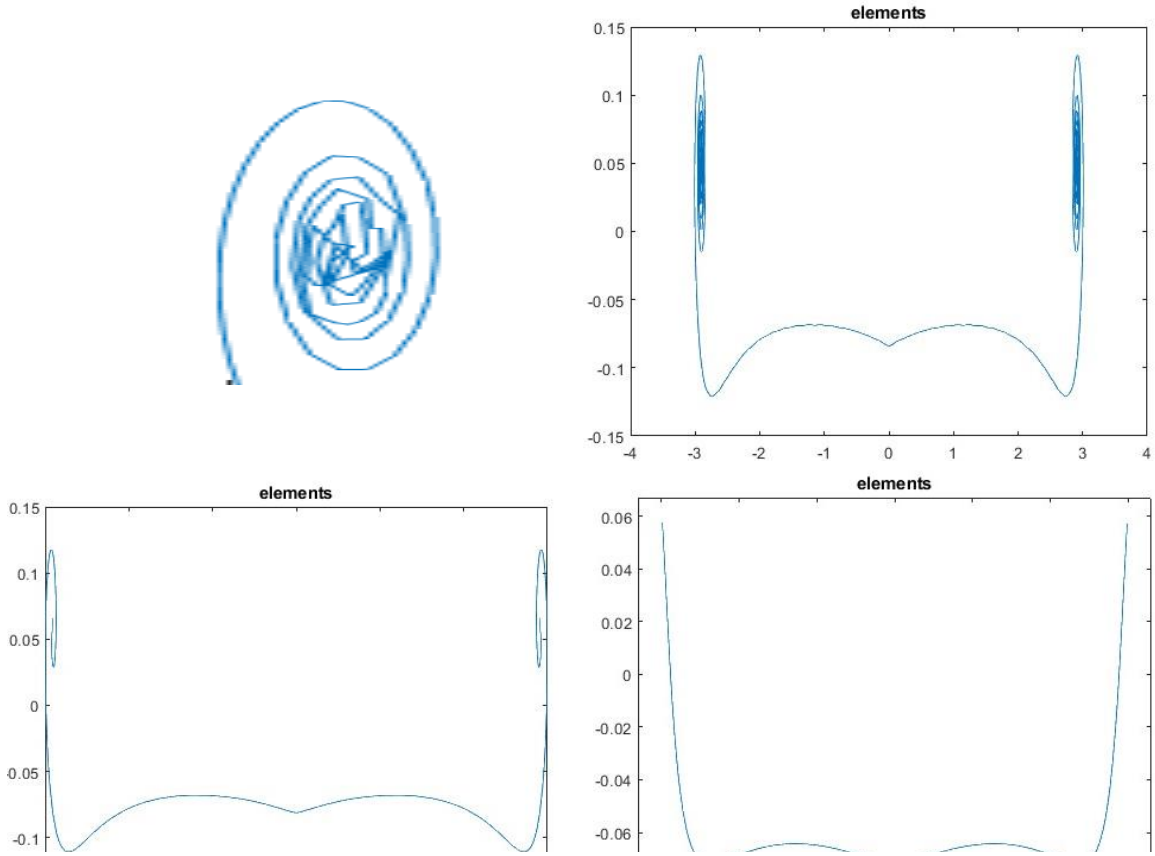

Figure 16(a) 16(b) 16(c) 16 (d) - The Unstable Vortex Core for SF1 = 0.005 (A), The Shape of the Wake for SF1 = 0.005 (B) SF1 = 0.05 (C) SF1 = 0.25 (D)

4.1.4. Smoothing Factor Analysis – Rear Wing

Table 6 - discretisation Parameters for SF2 Study

Parameter	Value	Unit
Timestep	0.001	Seconds
No Spatial Steps	400	N/A
Smoothing Factor – Front Wing	0.05	N/A

In this experiment, the impact of the smoothing factor for the induced velocity is investigated (SF2). The results presented in Figure 17, demonstrate that the total lift coefficient converges as the smoothing factor tends to zero. This outcome is consistent with the theoretical expectations, considering that the rear wing is placed far from the vortex's core and the effect of the smoothing factor is at its maximum when the points are closely spaced (as shown in Equation 14). These findings suggest that the smoothing factor for the induced velocity of the flow at a point should be determined based on its proximity to the vortex core, with it increasing as it gets closer.

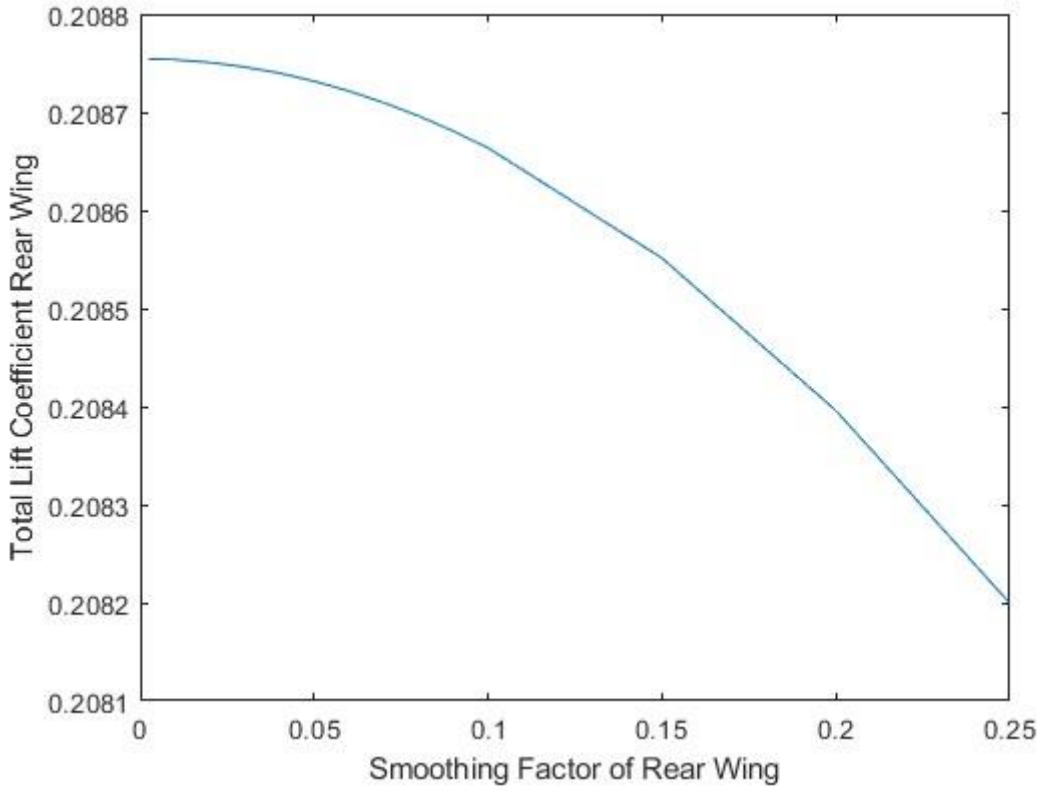

Figure 17 – Effect of SF2 on Rear Wing Total Lift Coefficient for Base Configuration

4.2. Replicating Physical Flow Properties

In order to recreate McAlister's experiments, discretisation parameters were chosen based upon the results of section 4.2. and are displayed in Table 7 alongside the wing dimensions and other relevant variables. As the previous section highlighted the importance of checking the shape of the rollup before commencing with experiments, with Figure 18 showing that the core of the vortex is stable and has a reasonable number of turns.

Table 7 - Parameters for NACA 0015 Study

Wing Dimensions	Value	Unit
Wingspan	3.423	m
Root Chord	0.52	m
Tip Chord	0.52	m
Area	1.785	m^2
Taper Ratio	1	N/A
General Parameters		
Freestream Velocity	46	ms^{-1}
Gap	0	m
Stagger	2.08	m
AOA	8	deg
Zero Lift AOA	0	deg
Discretisation Parameters		
No Spatial Steps	400	N/A
Timestep	0.001	N/A
Smoothing Factor – 1	0.05	N/A

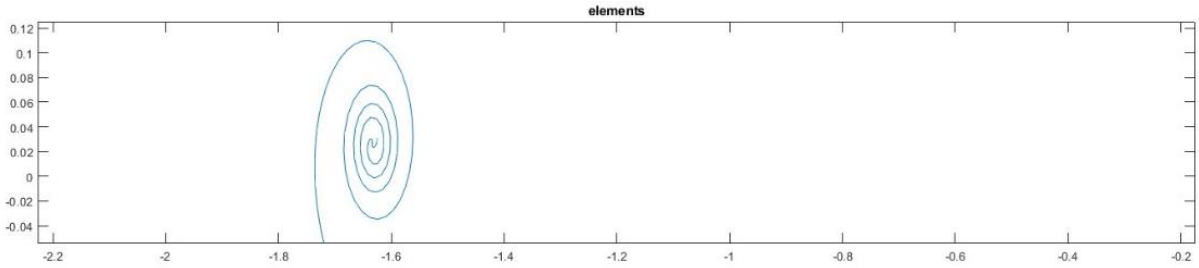

Figure 18 - Vortex Core For NACA 0012 Study

The present study conducted experiments to investigate the ratio of the vertical flow velocity to the free stream velocity, which is a crucial parameter affecting the performance of tandem wings. It was decided to compare against measurements taken at x/c=4, where the vortex core was observed to be level with the trailing edge of the airfoil. The selected angle of attack was 8 degrees, as it produces a high vorticity while remaining within the linear region of the NACA 0015 airfoil, thus ensuring the validity of the results. The experimental results are presented in Figure 19.

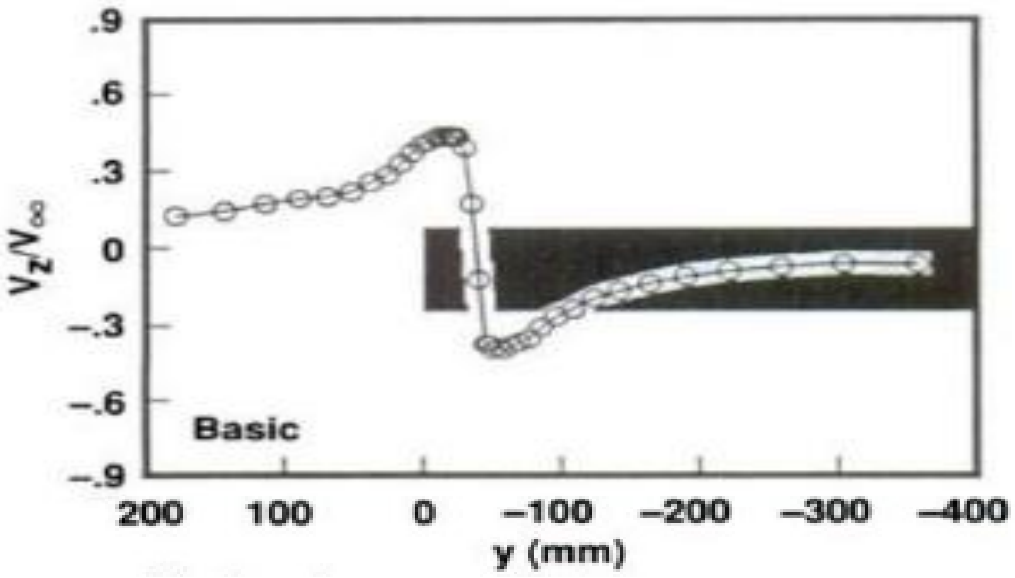

Figure 19 - Experimental Results for Vertical Velocity of NACA 0015 Wake

Experimentation with the model showed that so long as the model was stable, the timestep, number of point vortices and the smoothing factor in the rollup (SF1) had only a minor impact on the measurements recorded. However, the smoothing factor used in determining the velocity measurements (SF2) showed to have a huge impact. As they were investigated over the range of following values: 0.005, 0.01, 0.02, 0.03, 0.04, 0.05. In Figure 20, as the smoothing factor is increased the maximum velocity decreases and the radius of the core increases. Additionally, at small values the vortex no longer behaves as indicated in Rankines vortex model and local maxima form in the velocity measurements that are not located at the vortex core radius, this can be clearly seen in Figure 21. Finally, because beyond a certain point, decreasing the smoothing factor did not increase the maximum velocity the model could be achieved. Meaning it underestimated the maximum vertical velocity of the flow, although the donwash towards the wing root was correctly estimated.

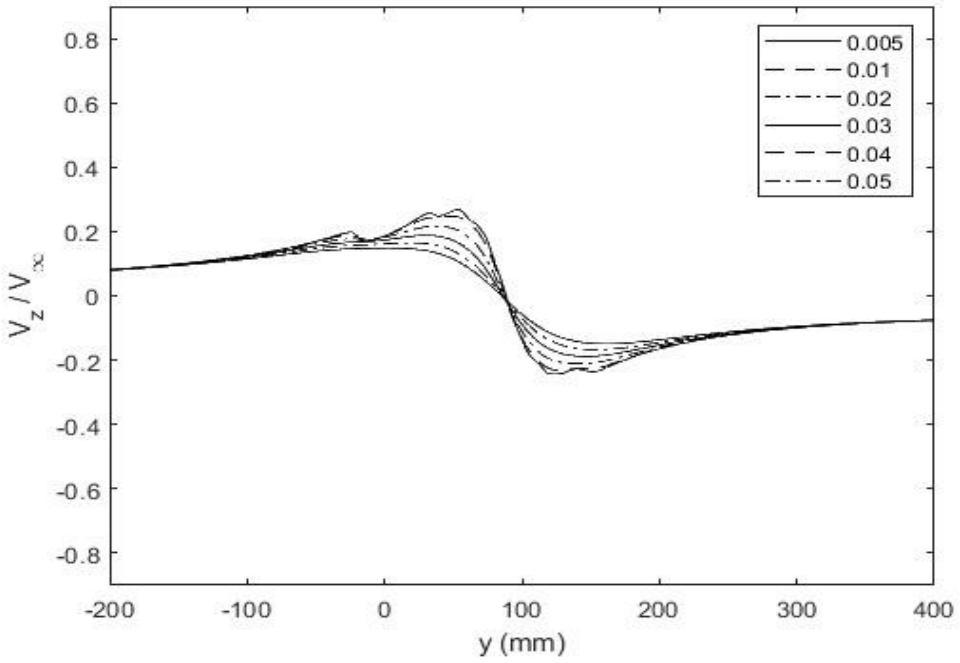

Figure 20 - VEM Vertical Velocity Centred About Experimental Core Position for NACA 0012 Study

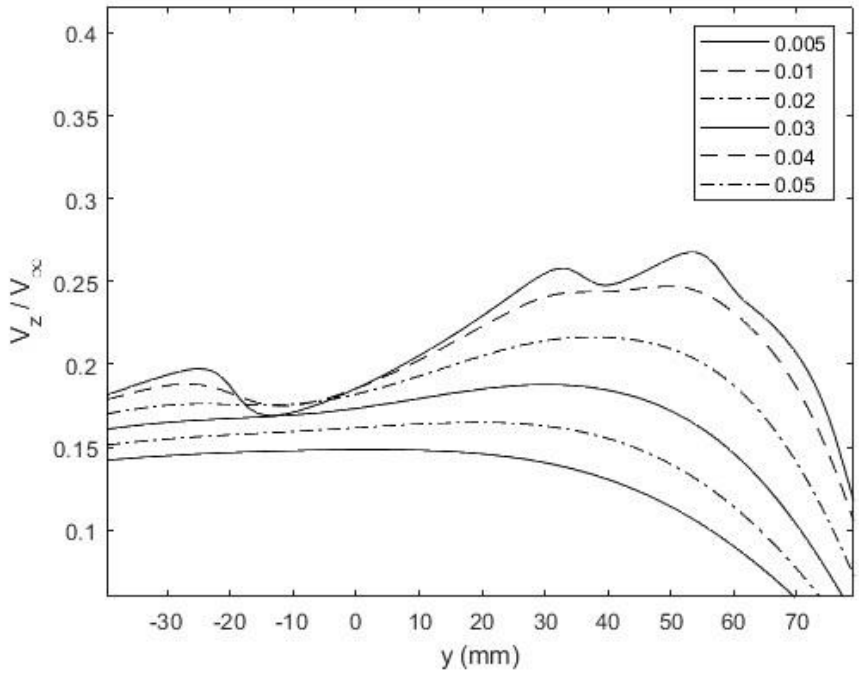

Figure 21 - Zoomed VEM Vertical Velocity Centred About Experimental Core Position for NACA 0012 Study

A major reason why the maximum vertical velocity could have been underestimated is that the results in Figure 20 are taken at where the core was in the experiment and not in the model, which was located above the wing instead of level with it. As such the experiment was repeated by setting the height where readings were taken at the height of the core (z_1), to see the behaviour through the core. Figures 22 and 23 show an increase in maximum velocity that brings it much closer in line with the experimental results, however the oscillatory behaviour was even more prevalent.

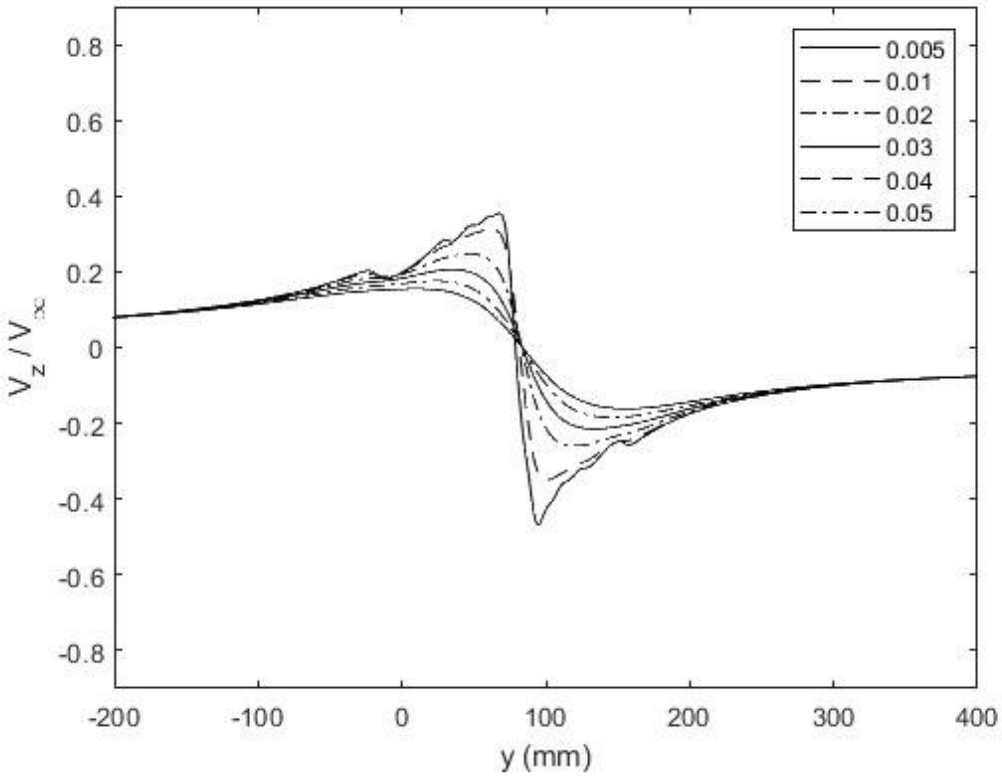

Figure 22 - VEM Vertical Velocity Centred About Calculated Core Position for NACA 0012 Study

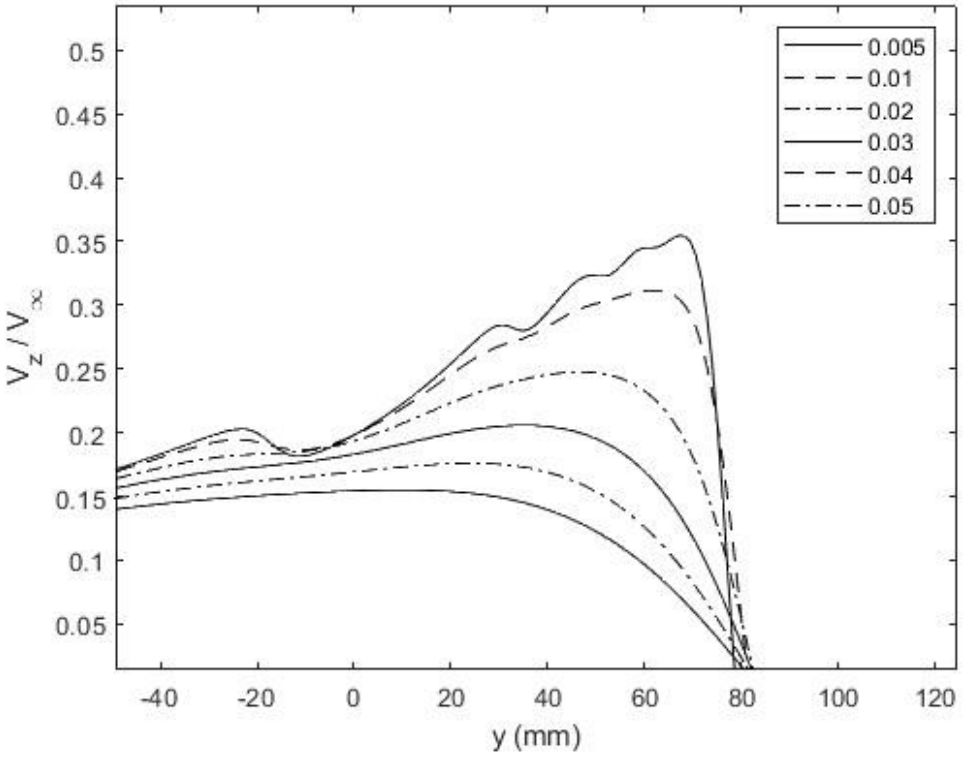

Figure 23 - Zoomed VEM Vertical Velocity Centred About Calculated Core Position for NACA 0012 Study

One reason for the oscillations is that the vortex only has 4 complete turns in the rollup and so there are significant gaps between the points of influence, causing troughs in the space between them. In order to see if this is the case the simulation was ran again with the following parameters $\Delta t = 0.0001,\ No\ Points = 1200\ \&\ SF_1 = 0.01$. This had a significantly larger run time but resulted in a greater number of turns, shown in Figure 24.

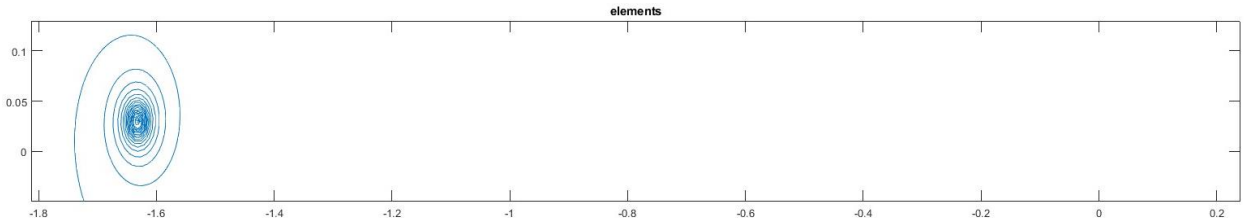

Figure 24 - Rollup for NACA 0015 High Resolution Study

This increased resolution acted to smooth the curve, however as shown in Figures 25 and 26 there is still a small level of oscillation, mostly centred around the outermost turn. As such this may be a consequence of the model that cannot be avoided unless unreasonably large resolutions are used, or an altered method is devised to find the induced velocity.

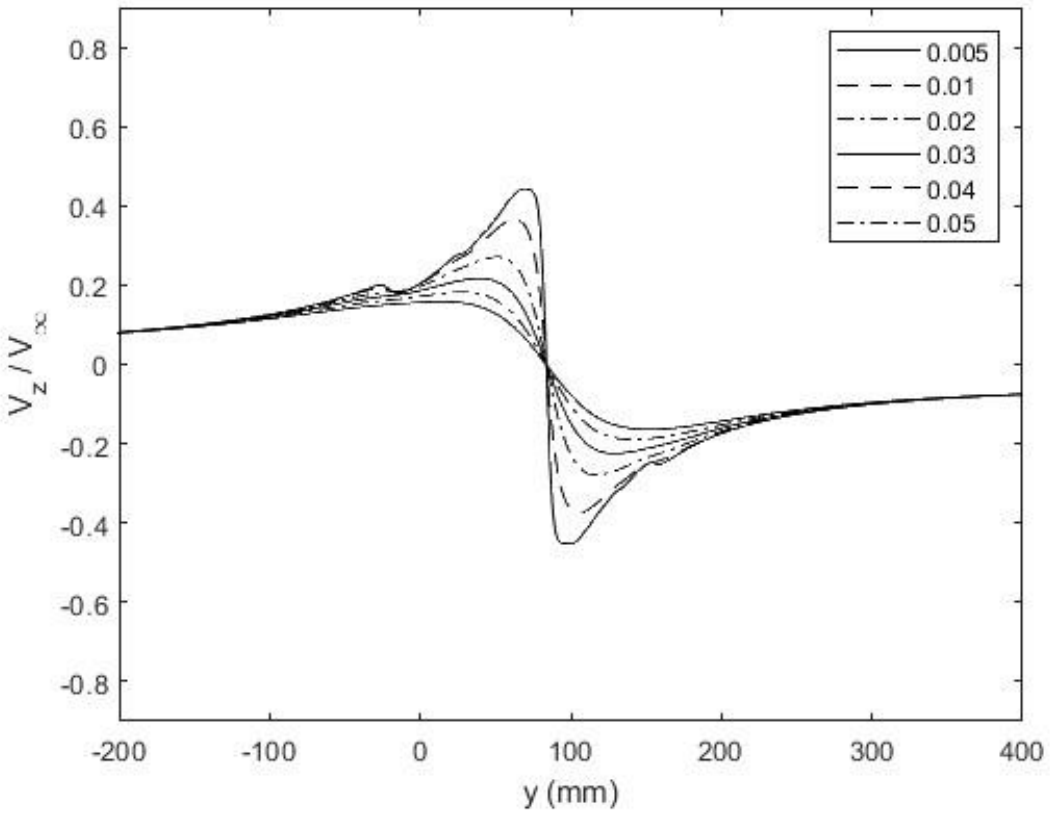

Figure 25 – VEM Vertical Velocity Centred About Calculated Core Position for NACA 0015High Resolution Study

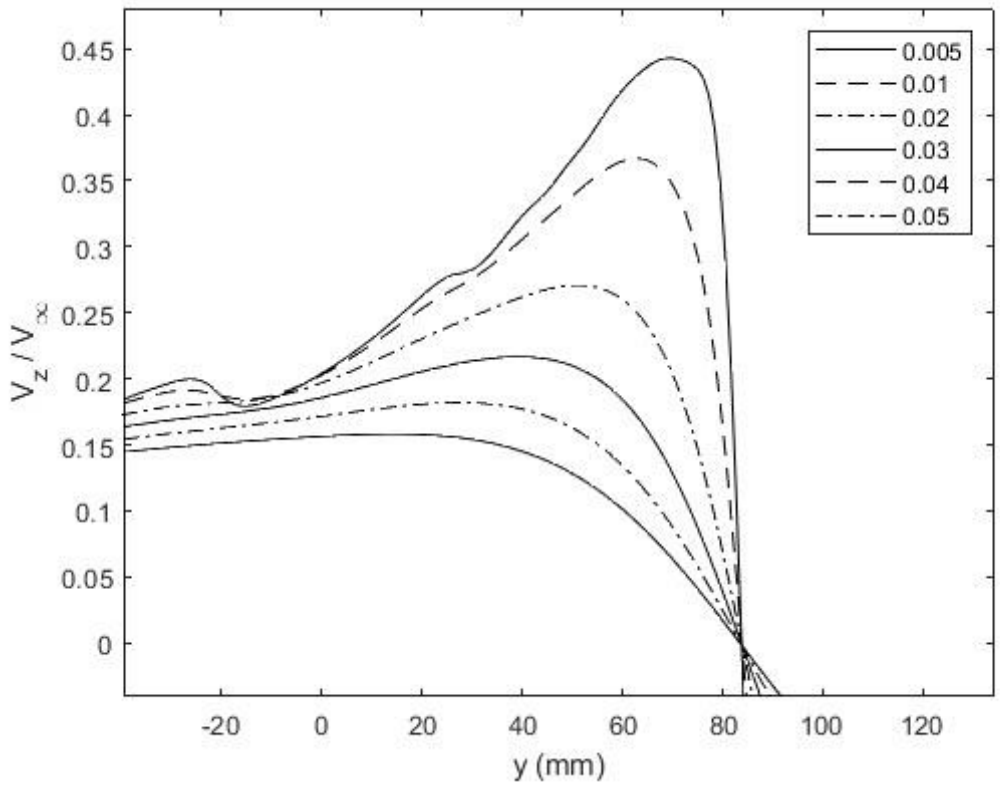

Figure 26 – Zoomed VEM Vertical Velocity Centred About Calculated Core Position for NACA 0015High Resolution Study

McAlisters Experiments investigated the movement of the centre of thevortex core as the wake evolved downstream. Figures 27 and 28 show that it moved inwards and downwards resepctively. Unfortunately the VEM showed very little movement in the position of the vortex core as evident in Figures 29 and 30. This is quite impactful as the greatest effects are seen in close proximity to the core and so if it its position is not accurately captured the most volatile effects will be improperly accounted for. Additionally the discrepency between experiment and simualtion cannot be attriubuted to factors such as the confinement error from the small wind tunnel. This is because the experimental results behaved as expected where as the simulation captured no movement.

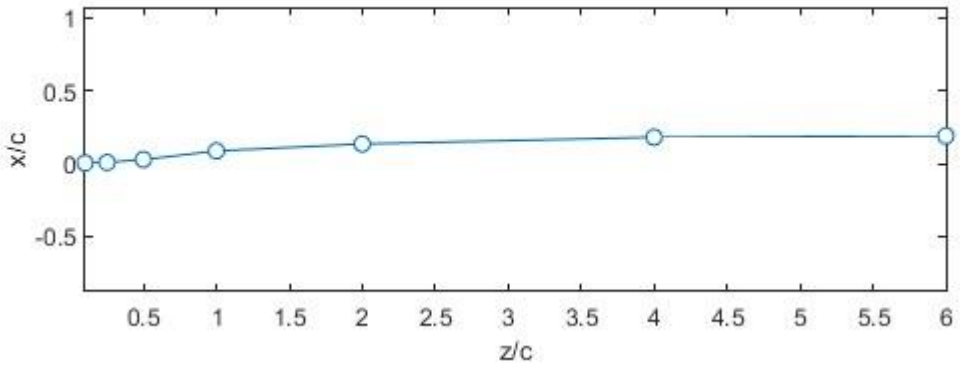

Figure 27 - Spanwise Displacement of Vortex Core From VEM

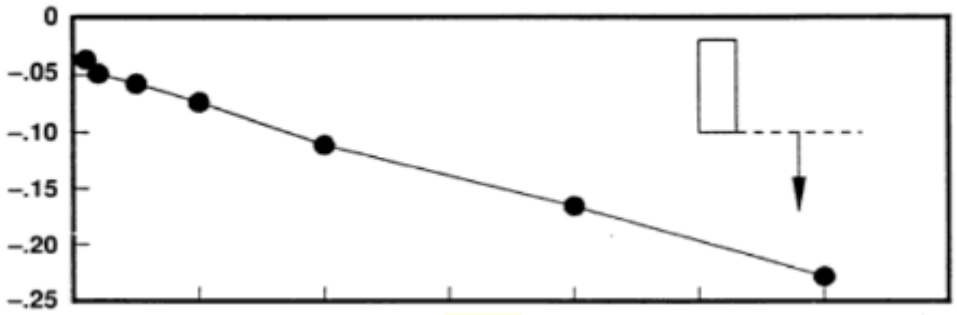

Figure 28 - Spanwise Displacement of Vortex Core From Experiment

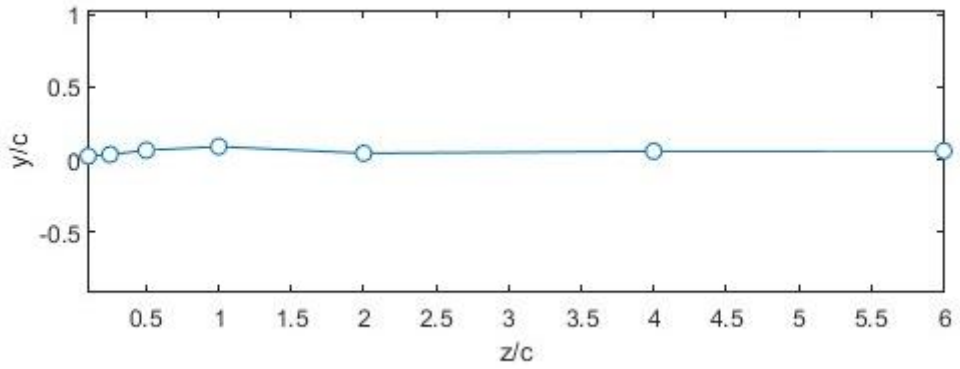

Figure 29 - Vertical Displacement of Vortex Core From VEM

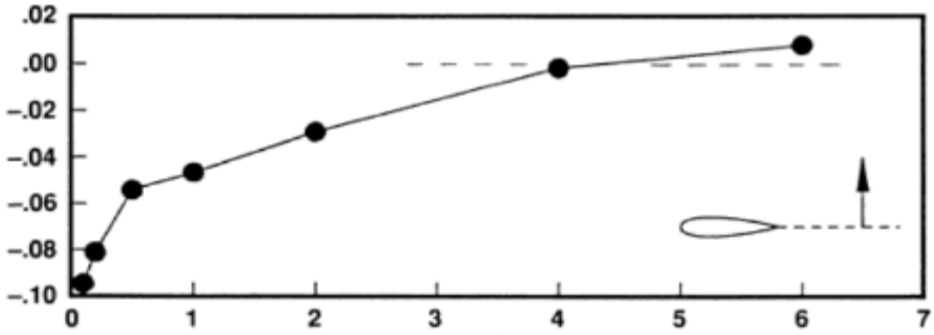

Figure 30 - Vertical Displacement of Vortex Core From Experiment

The Experimental results from the NACA 0012 were then recreated in the exact same manner as those for the NACA 0015, with the input parameters shown in Table 8. Additionally Figure 31 shows the core of the vortex is stable under these conditions.

Table 8 - Parameters for NACA 0012 Study

Wing Dimensions	Value	Unit
Wingspan	0.508	m
Root Chord	0.0762	m
Tip Chord	0.0762	m
Area	0.03871	m^2
Taper Ratio	1	N/A
General Parameters		
Freestream Velocity	8	ms^{-1}
Gap	-0.0556	m
Stagger	0.2438	m
AOA	10	deg
Zero Lift AOA	0	deg
Discretisation Parameters		
No Spatial Steps	600	N/A
Timestep	0.00005	N/A
Smoothing Factor – 1	0.0025	N/A

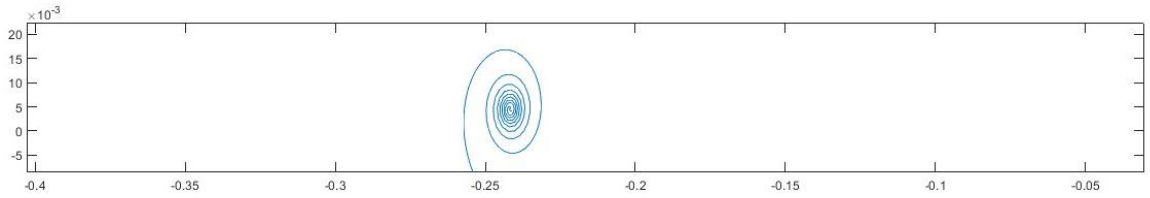

Figure 31 - Rollup of Vortex for NACA 0012 Study

Unfortunately, an even larger gap between the results seen in between the experiment and simulation, as shown in Figures 32 and 33. On top of achieving a much smaller vertical velocity even at the smallest smoothing factor, the downwash at the wing root was also greatly under estimated. However, the confinement error may be much greater in this experiment as the cross-sectional area of the flow compared to the wing was even low than the NACA 0015 experiments.

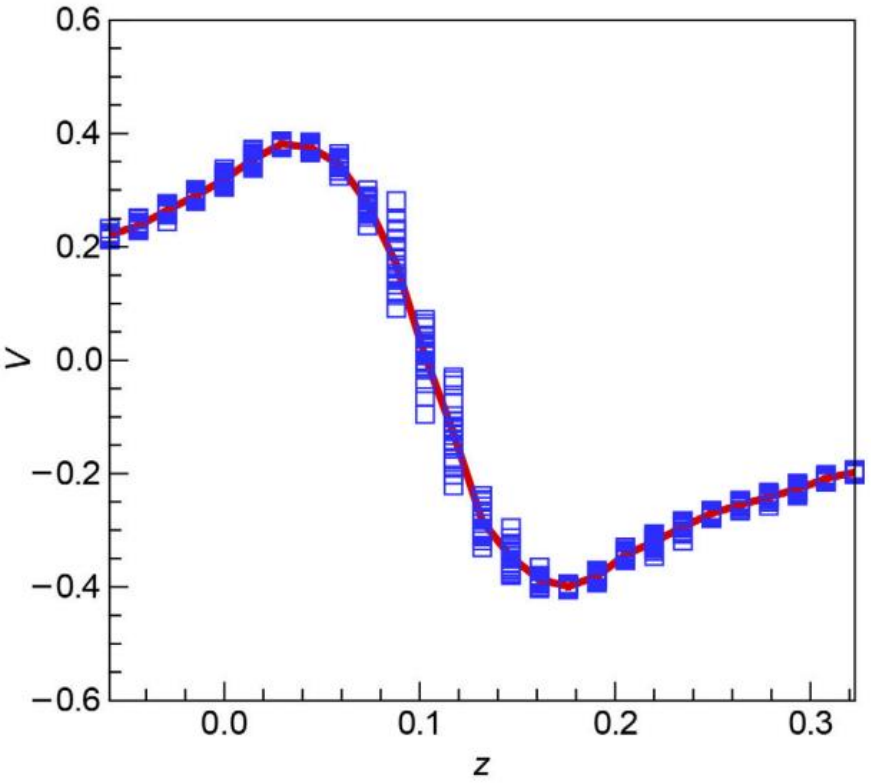

Figure 32 - Experimental Results for Vertical Velocity of NACA 0012 Wake

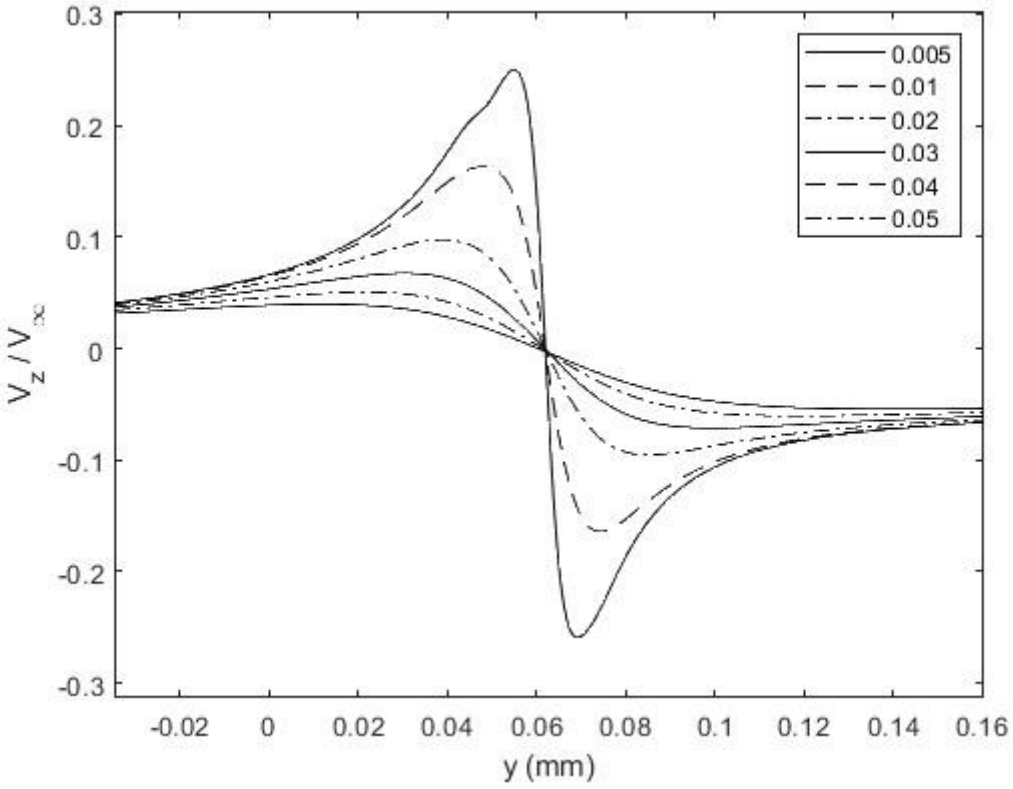

Figure 33 - VEM Vertical Velocity Centred About Calculated Core Position for NACA 0012 Study

4.3. Tandem Wing Pitch Investigation

This study aims to investigate the behaviour of a tandem wing aircraft in pitch by assessing the lift coefficient of the rear wing for two nose-up pitch rates, 1 deg/s and 2 deg/s. The results, as shown in Figures 34 and 35, indicate that no random or chaotic behaviour was observed, and instead, there was an almost constant difference between the dynamic and static cases. This suggests that the difference could be due to the pitch rate inducing a slightly different effective angle on each wing, and the magnitude of this effect would be mostly constant. However, further examination of Figures 36 and 37 shows that there is a greater reduction in lift coefficient for the higher pitching rate. Furthermore, the upward curve in both these figures could indicate that as the angle increases, the stronger vortex may gain influence. Therefore, it can be concluded that the pitch rate has a significant effect on the lift coefficient of the rear wing, and this effect is more prominent at higher pitch rates.

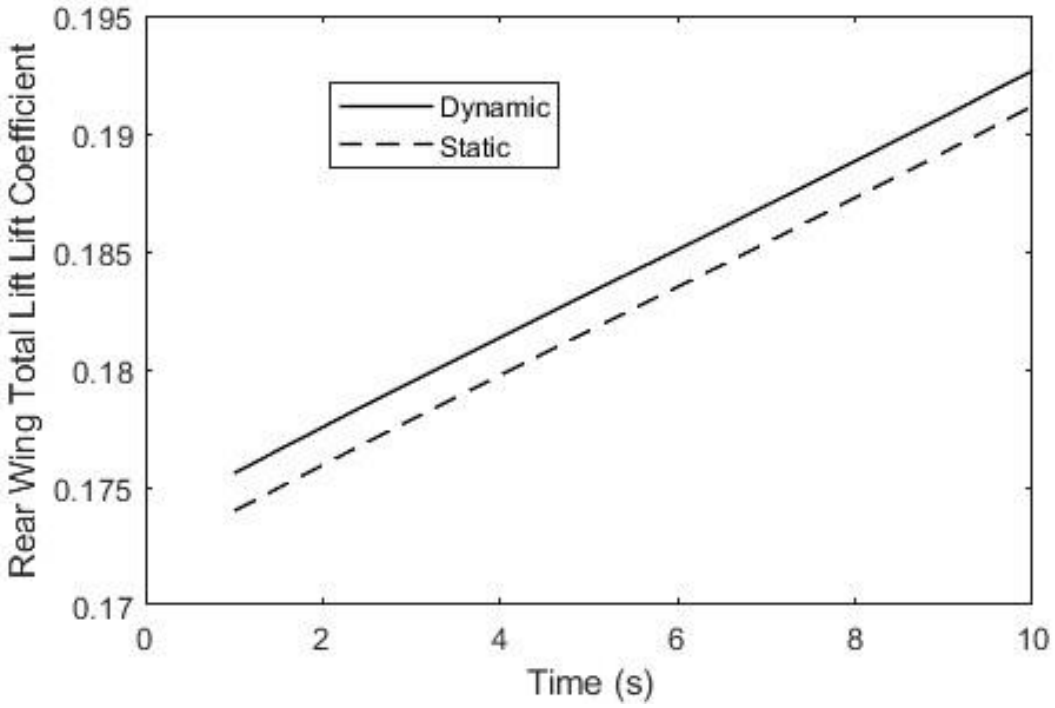

Figure 34 - Rear Wing Lift Coefficient Over Time for Pitch Rate of 1 deg/s

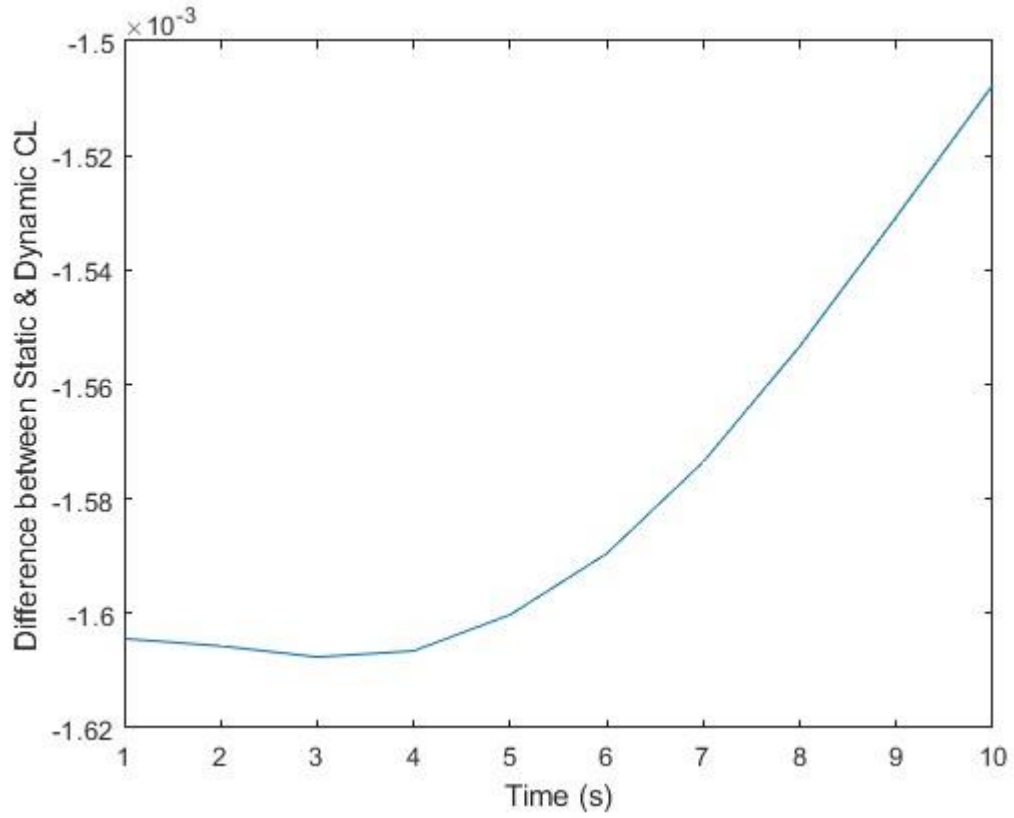

Figure 35 – Difference Between Static and Dynamic Rear Wing Lift Coefficient Over Time for Pitch Rate of 1 deg/s

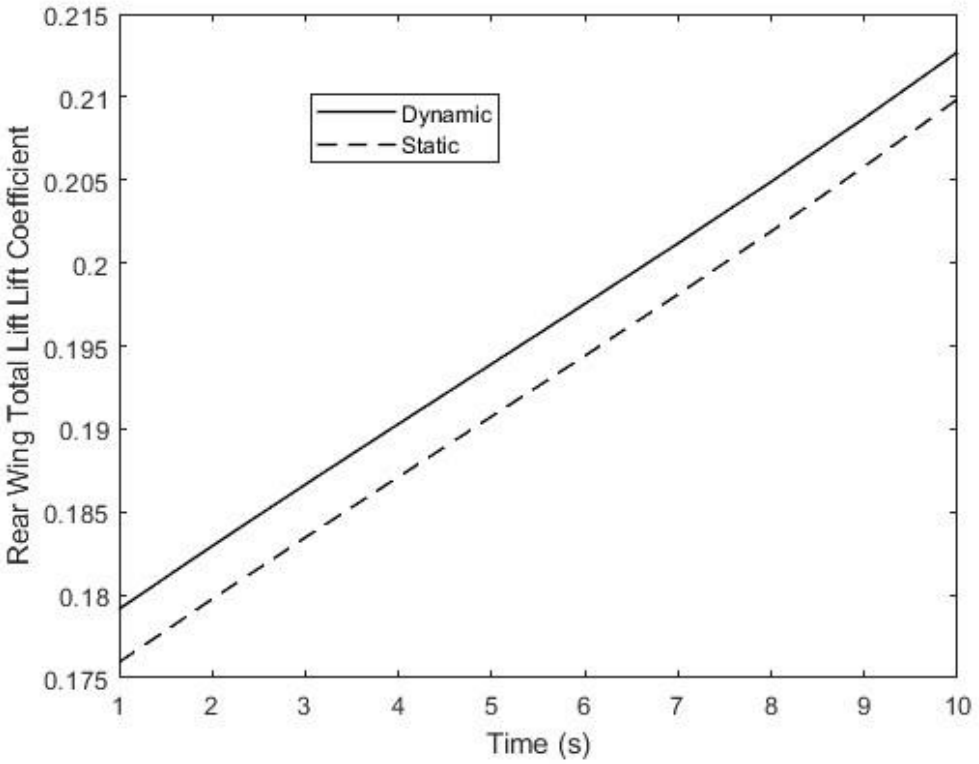

Figure 36 Figure 34 - Rear Wing Lift Coefficient Over Time for Pitch Rate of 2 deg/s

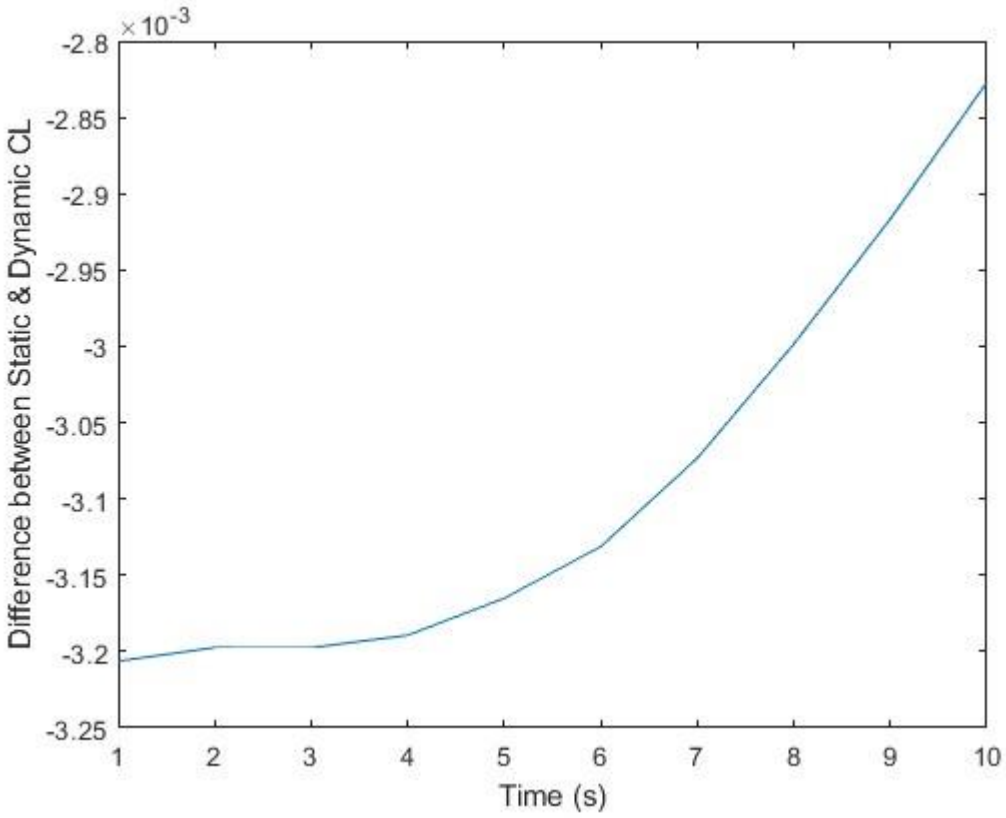

Figure 37 - Difference Between Static and Dynamic Rear Wing Lift Coefficient Over Time for Pitch Rate of 2 deg/s

5. DISCUSSION

The results of the sensitivity indicate that the VEM could achieve stable results, even if the discretisation parameters are set at relatively low resolutions. Furthermore, it was found that so long as the wake rollup remains stable, the impact of discretisation parameter resolution on the total lift coefficient of the rear wing and the behaviour of the wake rollup is minimal. This is especially promising as numerical methods such as the VEM are typically employed in early-stage aircraft design, where a high degree of accuracy is not always necessary. Thus, lower resolutions such as those highlighted in the sensitivity studies, can provide the required level of accuracy, and offer faster run times for simulations. Whilst the present study only examined a single design configuration and so further exploration is required, the findings are significant. This is because the literature review identified the potential advantage of the VEM its ability to provide some of the functionality of traditional CFD but it is much simpler and quicker to use. Therefore by showing that the VEM can produce accurate results with limited computational resources, this study indicates that it has the potential to be a promising tool in aircraft design.

The next part of the study aimed to investigate the VEMs ability to replicate experimental flows. The comparison between simulated and experimental results indicated that the VEM can reasonably replicate experimental flows, but with some drawbacks. Firstly, the induced velocities of the experiments could not be perfectly replicated even at high resolutions and low scale factors. Moreover, the estimation of an appropriate smoothing factor needs to be established and subsequently verified to trust the results without experimental validation due to the significant effect caused by changing SF2. However, it is worth noting that the VEM was not capable of accurately tracking the position of vortex cores, and thus it is only useful in predicting flow regions that are not in close proximity to the core. Furthermore, in order to properly test the VEM, experimental results in

unconfined conditions would be needed as the confinement issues of the experiments used may have a larger impact than predicted leading to non-replicable results.

A preliminary investigation was undertaken to explore the dynamics of a tandem wing aircraft in pitch. The use of the VEM in modelling dynamic flow behaviour was demonstrated as a promising approach, despite the lack of experimental results to validate these simulations. Therefore, it is uncertain whether the simulated behaviour accurately represents real-life scenarios, however the results presented in this investigation appeared reasonable. Additionally, the relationship between pitch rate and rear wing lift coefficient was found to be relatively simple, which gives hope for designing control systems for a tandem wing aircraft, at least in pitch. Nonetheless, further research is needed to confirm the findings of this investigation, and experimental validation is essential to ensure the reliability of the modelling approach used.

6. CONCLUSIONS

The first and most basic aim of this study was to use the VEM to create a model that could be used to track the development of the wake of an aircraft. Initial research showed that the most appropriate way of modelling the flow was as a 2D initial value problem in the Trefftz plane. This solution provided a method that was accurate, efficient, and highly adaptable. However, it is only valid for unseparated flow within the intermediate region of an aircraft's wake.

The discretisation parameters of this method were the timestep, number of vortex bearing points and a smoothing factor to avoid singularities. It was found that the timestep and number of point vortices converged on an accurate answer at relatively low resolutions, this is important as it means accurate simulations can be executed at very high speeds. The Major finding was that as the smoothing factor tended to zero, the number of turns in the vortex and thus accuracy of the results increased. However, as the smoothing factor was reduced the solution became unstable and gave erroneous results. But, it was found that by increasing the resolution of the other parameters, stability could be achieved for lower smoothing factors.

Following on from this, an attempt was made to validate the method against experimental results. Limited data in the literature meant that the only useful data to compare against was the downwash induced by the tip vortex, across a spanwise set of points downstream. This proved to be useful and the method produced results that exhibited similar velocity profiles, however it did struggle to accurately replicate the movement of the vortex core. However the key finding was that the smoothing factor used to calculate the induced velocity had a huge impact on the velocity at the core radius and so further work is needed to deduce a method to select an appropriate value prior to each experiment.

Finally, the dynamic behaviour of a tandem wing aircraft in pitch was investigated using the method. Preliminary results indicated that the behaviour in pitch should be of little concern as they displayed a near linear behaviour.

7. REFERENCES

[1] D. J. Acheson, Elementary Fluid Dynamics, Clarendon Press, 1990.

[2] T. H. I. K. Md. Shahjahan Ali, “Unsteady RANS and LES Simulation of an Ideal Rankine Vortex Decay,” *Advances in Civil Engineering,* 2012.

[3] German Federal Bureau of Aircraft Accident Investigation, “Interim Report BFU17-0024-2X,” Bundesstelle für Flugunfalluntersuchung, 2017.

[4] T. Sarpkaya, “Vortex Element Methods for Flow Simulation,” *Advances in Applied Mechanics,* vol. 31, pp. 113-247, 1994.

[5] I. M. V.S. Morevallia, “Vortex element method for 2D flow simulation with tangent velocity components on airfoil surface,” 2012.

[6] A. Minardo, “The Tandem Wing: Theory, Experiments, and Practical Realisations,” POLITECNICO DI MILANO, Milan, 2014.

[7] E. Gideon, “Rutan quickie,” [Online]. Available: https://commons.wikimedia.org/wiki/File:Rutan_quickie_q2.jpg. [Accessed 16 04 2023].

[8] I. Kryvokhatko, Aerodynamics of Tandem Wing Aircraft: From Dinosaurs to UAVs and Supersonic Planes, Springer, 2023.

[9] N/A, “Arab Military Industries,” [Online]. Available: https://army.alafdal.net/t121310p15-topic. [Accessed 15 04 2023].

[10] Lilium, “Lilium begins flight testing in Spain,” Lilium, 04 April 2022. [Online]. Available: https://lilium.com/newsroom-detail/lilium-begins-flight-testing-in-spain. [Accessed 16 April 2023].

[11] L. Blain, “Lilium's weird, energy-hungry "small fan" design could be a hidden ace,” New Atlas, 09 June 2021. [Online]. Available: https://newatlas.com/aircraft/lilium-interview-small-fans-pros-cons/. [Accessed 16 April 2023].

[12] J. D. Anderson, Fundamentals Of Aerodynamics 5th Edition, Chicago: McGraw-Hill, 2011.

[13] T. F. J. K. T. T. H. A. Shekarriz, “Near-Field Behavior of a Tip Vortex,” *AIAA JOURNAL,* vol. 31, no. 1, pp. 112-118, 1993.

[14] J. R. B. J. M. V. F. O. d. A. Leandro J.L. Stival a b Leandro J.L. Stival, “Wake modeling and simulation of an experimental wind turbine using large eddy simulation coupled with immersed boundary method alongside a dynamic adaptive mesh refinement,” *Energy Conversion and Management,* vol. 268, pp. 1-16, 2022.

[15] T. L. F. M. F. K. D. Birch, “Rollup and Near-Field Behavior of a Tip Vortex,” *J. AIRCRAFT,* vol. 40, no. 3, pp. 603-607, 1992.

[16] F. H. D. D. Thomas Gerz, “Commercial aircraft wake vortices,” *Progress in Aerospace Sciences ,* vol. 38, no. 1, pp. 181-208, 2002.

[17] B. N. Shashikanth, “Dissipative N-point-vortex Models in the Plane,” *Journal of Nonlinear Science,* vol. 20, pp. 81-103, 2009.

[18] M. H. D. K. J. D.-M. M. H. a. D. K. Jennifer Dacles-Mariani, “Prediction of wake-vortex flow in the near- and intermediate-fields behind wings,” in *35th Aerospace Sciences Meeting and Exhibit*, Reno, 1997.

[19] W. H. M. Cheolheui Han, “Inviscid Wing-Tip Vortex Behavior Behind Wings in Close Formation Flight,” *JOURNAL OF AIRCRAFT,* vol. 42, no. 3, pp. 787-788, 2005.

[20] M. J. A W Bloy, “Lateral and directional stability and control in air-to-air refuelling,” *Proceedings of the Institution of Mechanical Engineers,* vol. 209, no. 1, pp. 299-305, 1995.

[21] M. G. W. A. W. Bloy, “Interference between tanker wing wake with roll-up and receiver aircraft,” *Journal of Aircraft,* vol. 31, no. 5, pp. 1214-1221, 2012.

[22] J. C. Cheolheui Han, “Unsteady Trailing Vortex Evolution Behind a Wing in Ground Effect,” *JOURNAL OF AIRCRAFT,* vol. 42, no. 2, pp. 429-434, 2005.

[23] D. F. P. G. E. C. L. Jacquin, “The properties of a transport aircraft wake in the extended near field - An experimental study,” in *39th Aerospace Sciences Meeting and Exhibit*, Reno, 2012.

[24] D. H. R. S. R. P. D. H. R. S. R. Perry, “NASA wake vortex research for aircraft spacing,” in *35th Aerospace Sciences Meeting and Exhibit*, Reno, 1997.

[25] V. B. F. H. S. R. I.N. Smalikho, “Method of radial velocities for the estimation of aircraft wake vortex parameters from data measured by coherent Doppler lidar,” *Optics Express,* vol. 23, no. 19, pp. 1194-1207, 2015.

[26] T. P. Alexandre Corjon, “Vortex model to define safe aircraft separation distances,” *Journal of Aircraft,* vol. 33, no. 3, pp. 547-556, 1996.

[27] F. Holzäpfel, “Probabilistic Two-Phase Wake Vortex Decay and Transport Model,” *Journal of Aircraft,* vol. 40, no. 2, pp. 323-330, 2003.

[28] ADVISORY GROUP FOR AEROSPACE RESEARCH & DEVELOPMENT, “The Characterisation & Modification of Wakes from Lifting Vehicles in Fluids,” in *Fluid Dynamics Panel Symposium*, Trondheim, 1996.

[29] F. H. James N. Hallock, “A review of recent wake vortex research for increasing airport capacity,” *Progress in Aerospace Sciences,* vol. 98, pp. 27-36, 2018.

[30] captron, “Can Planes Crash from Turbulence?,” fearless flight, 01 December 2010. [Online]. Available: https://fearlessflight.com/can-planes-crash-from-turbulence/. [Accessed 15 April 2023].

[31] K. V. S. L.Hariramakrishnan, “CFD ANALYSIS OF TANDEM WINGED AIRCRAFT,” *International Journal of Engineering Research and Reviews,* vol. 5, no. 1, pp. 1-6, 2017.

[32] M. Z. A. T. C. Y. Z. Husain, “Two-dimensional analysis of tandem/staggered airfoils using computational fluid dynamics,” *International Journal of Mechanical Engineering Education ,* vol. 33, no. 3, pp. 195-207.

[33] S. O. Taskin Kaya, “Aerodynamic Design and Control of Tandem Wing UAV,” in *AIAA Aviation 2019 Forum*, Dallas, 2019.

[34] N. S. K. S. O. A. M. A. M. T S Sugandi, “Prediction of static stability in tandem wing unmanned aerial vehicle,” in *Journal of Physics: Conference Series*, Jakarta, 2018.

[35] H. W. Hoa Cheng, “Prediction of Lift Coefficient for Tandem Wing Configuration or Multiple-Lifting-Surface System Using Prandtl’s Lifting-Line Theory,” *International Journal of Aerospace Engineering,* vol. 2018, pp. 1-15, 2018.

[36] A. P. J. Katz, Low-speed aerodynamics: from wing theory to panel methods, McGraw-Hill Education, 2001.

[37] D. H. P. S. I. Lashgari, “A numerical study of the flow around a circular cylinder at high Reynolds numbers,” *Journal of Fluid Mechanics,* vol. 730, no. 1, pp. 596-623, 2013.

[38] W. L. Y. C. L. Y. Xie Changchuan, “Static aeroelastic analysis of very flexible wings based on non-planar vortex lattice method,” *chinese journal of aeronautics,* vol. 26, no. 3, pp. 514-521, 2013.

[39] R. P. J. M. R. G. J. Murua, “Applications of the unsteady vortex-lattice method in aircraft aeroelasticity and flight dynamics,” *Progress in Aerospace Sciences,* vol. 55, pp. 46-72, 2012.

[40] A. Z. A.S. Ginevsky, Vortex wakes of Aircrafts, Springer, 2009.

[41] R. Krasny, “Computation of vortex sheet roll-up in the Trefftz plane,” *Journal of Fluid Mechanics,* vol. 184, no. 1, pp. 123-155, 1987.

[42] N. Polaczyk, E. Trombino, P. Wei and M. Mitici, “A review of current technology and research in urban on-demand air mobility applications,” in *8th Biennial Autonomous VTOL Technical Meeting and 6th Annual Electric VTOL Symposium 2019*, Delft, 2019.

[43] C. C. Alessandro Bacchini, “Electric VTOL Configurations Comparison,” Department of Mechanical and Aerospace Engineering, Politecnico di Torino, Turin, 2019.

[44] W. F. Phillips, “Lifting-Line Analysis for Twisted Wings and Washout-Optimized Wings,” *Journal of Aircraft,* vol. 41, no. 1, pp. 128-136, 2004.

[45] R. J. LeVeque, Finite Difference Methods for Ordinary and Partial Differential Equations, Society for Industrial and Applied Mathematics, 2007.

[46] R. K. T. K. W. McAlister, NACA 0015 Wing Pressure and Trailing Vortex Measurements, NASA, 1991.

[47] A. F. F. M. R. M. K.B.M.Q. Zaman, “An Experimental Study and Database for Tip Vortex Flow From An Airfoil,” NASA, Cleveland, 2017.

[48] M. Figat, “A strategy of the longitudinal control for the tandem wing configuration design,” *Aircraft Engineering and Aerospace Technology,* vol. 95, no. 1, pp. 155-169, 2023.

[49] B. Fornberg, A Practical Guide to Pseudospectral Methods, Cambridge University Press, 1996.

[50] A. F. F. a. M. R. M. K.B.M.Q. Zaman.

8. APPENDICES

8.1. Appendix A - Classic LLT Code (LLT_1.m)

```
function [Cl] = LLT_1_rear(b_2, area_2, TR_2, NoLocations_2, alpha_2,
alpha01_2, Airspeed, WingLocation_1 );
a0_2 = 2*pi;
%b = 20;
%area = 0.4;
%TR = 0.5%0:0.01:1;
SizeTR = size(TR_2);
Croot = zeros(1,SizeTR(2));
Ctip = zeros(1,SizeTR(2));
for n = 1:SizeTR(2)
Croot(1,n) = 2*area_2/(b_2*(TR_2(1,n)+1));
Ctip(1,n) = TR_2(1,n)*Croot(1,n);
end
%alpha01 = 0;
%alpha = 4;
alpha_2 = alpha_2*(pi/180);
alpha01_2 = alpha01_2*(pi/180);
rho = 1.225;
%NoLocations = 100;
NoAValues = 50;
%Airspeed = 67;
Cl = zeros(SizeTR(2),1);
Cdi = zeros(SizeTR(2),1);
LocalWingLoading = zeros  (100,1);
for n11 = 1:SizeTR(2)
% Convert AOA & zero lift angle to rad
% Create Working Matricies
LHS = zeros (NoLocations_2,1);
RHS = zeros(NoLocations_2,NoAValues);
theta = zeros(NoLocations_2,1);
C = zeros(NoLocations_2,1);
% Create wing locations converted to sine form
WingLocation = zeros(NoLocations_2,1);
for n = 1 : NoLocations_2
    WingLocation(n) = WingLocation_1(n);
    theta(n) = acos (2*WingLocation(n)/b_2);
end

% Chord at wing position

for n1 = 1:NoLocations_2
    C(n1) = Ctip(n11)+(Croot(n11)-Ctip(n11))*(1+2*WingLocation(n1)/b_2);
```

```
    %C(n1) = (TR(1,n11) + ((n1/NoLocations)*(1-TR(1,n11))))*Croot(1,n11);
end
% Define LHS of equation

for n2 = 1:NoLocations_2
    LHS(n2) = pi*(alpha_2-alpha01_2)*C(n2)/(2*b_2);
end
% Define RHS of equation
for n3 = 1:NoLocations_2
    for m = 1:2:(2*NoAValues)-1
        RHS(n3,(m+1)/2) =
sin(m*theta(n3))*(1+(m*pi*C(n3)/(2*b_2*sin(theta(n3)))));
    end
end
A = RHS\LHS;
Croot(n11);
A(1);
Cl(n11) = ( b_2^2/area_2 ) * pi * A(1);

AnA1 = zeros(NoAValues,1);
for n4 = 1:NoAValues
    AnA1(n4) = (2*n4-1)*(A(n4)/A(1))^2;
end

% Find the Local Circulation & subsequently local Cl
AnSinNTheta = zeros(NoLocations_2,NoAValues);
SumAnSinNTheta = zeros(NoLocations_2,1);
LocalCirculation = zeros(NoLocations_2,1);
LocalCl = zeros(NoLocations_2,1);
for n4 = 1:NoLocations_2
    for m1 = 1:NoAValues
        AnSinNTheta (n4,m1) = A(m1)*sin((2*m1-1)*theta(n4));
    end
    SumAnSinNTheta(n4,1) = sum(AnSinNTheta(n4,:));
    LocalCirculation(n4,1) = 2*b_2*Airspeed*SumAnSinNTheta(n4,1);
    LocalCl(n4,1) = 2*LocalCirculation(n4,1)/(Airspeed*C(n4));
    LL(n4,1) = LocalCl(n4,1) * C(n4);
end
plot(WingLocation,LocalCl)

Cdi(n11) = sum(AnA1)*pi*(b_2^2/area_2)*A(1)^2;
%DPolar = zeros(SizeTR(2),1);
Dpolar(n11,1) = Cdi(n11)/(Cl(n11)^2);
%LD =zeros(SizeTR(2),1);
LD(n11) = 1 / Dpolar(n11)*0.8;
%for n34 = 1:100
%LocalWingLoading(n34) =
rho*Airspeed*LocalCirculation(n34);%LocalCl(n34)*C(n34);
%end
LocalCl;
%plot(WingLocation,LocalWingLoading)
xoxoxo = Cl
Cdi;
LD;
%waitforbuttonpress
end
plot(WingLocation,LocalCl)
%plot(TR,LD)
```

```
106.
107.Cl
```

107.1. Appendix B – Twisted LLT Code (LLT_2_twist.m)

```
108.function [Cl] = LLT_2_twist(b_2, area_2, TR_2, NoLocations_2, alpha_2,
    alpha01_2, Airspeed, WingLocation_1 );
109.a0_2 = 2*pi;
110.%b = 20;
111.%area = 0.4;
112.%TR = 0.5%0:0.01:1;
113.SizeTR = size(TR_2);
114.Croot = zeros(1,SizeTR(2));
115.Ctip = zeros(1,SizeTR(2));
116.for n = 1:SizeTR(2)
117.Croot(1,n) = 2*area_2/(b_2*(TR_2(1,n)+1));
118.Ctip(1,n) = TR_2(1,n)*Croot(1,n);
119.end
120.%alpha01 = 0;
121.%alpha = 4;
122.alpha_2 = alpha_2*(pi/180);
123.alpha01_2 = alpha01_2*(pi/180);
124.rho = 1.225;
125.%NoLocations = 100;
126.NoAValues = 50;
127.%Airspeed = 67;
128.Cl = zeros(SizeTR(2),1);
129.Cdi = zeros(SizeTR(2),1);
130.LocalWingLoading = zeros  (100,1);
131.for n11 = 1:SizeTR(2)
132.% Convert AOA & zero lift angle to rad
133.% Create Working Matricies
134.LHS = zeros (NoLocations_2,1);
135.RHS = zeros(NoLocations_2,NoAValues);
136.theta = zeros(NoLocations_2,1);
137.C = zeros(NoLocations_2,1);
138.% Create wing locations converted to sine form
139.WingLocation = zeros(NoLocations_2,1);
140.for n = 1 : NoLocations_2
141.    WingLocation(n) = WingLocation_1(n);
142.    theta(n) = acos (2*WingLocation(n)/b_2);
143.end
144.
145.% Define Omega
146.alpha_root = max(alpha_2);
147.alpha_ref = min(alpha_2);
148.omega = alpha_root-alpha_ref;
149.
150.% Chord at wing position
151.for n1 = 1:NoLocations_2
152.    C(n1) = Ctip(n11)+(Croot(n11)-Ctip(n11))*(1+2*WingLocation(n1)/b_2);
153.    %C(n1) = (TR(1,n11) + ((n1/NoLocations)*(1-TR(1,n11))))*Croot(1,n11);
154.end
155.% Define LHS of equation
156.% noting LHS_b = epsilon
157.
158.for n2 = 1:NoLocations_2
```

```
    LHS_a(n2) = 1;
    LHS_b(n2) = (alpha_2(n2)-alpha_root)/(alpha_ref-alpha_root);
end
% Define RHS of equation
for n3 = 1:NoLocations_2
    for m = 1:2:(2*NoAValues)-1
        RHS(n3,(m+1)/2) =
   sin(m*theta(n3))*(((2*b_2)/(pi*C(n3)))+(m/sin(theta(n3))));
    end
end
LHS_a = transpose(LHS_a);
LHS_b = transpose(LHS_b);
a = RHS\LHS_a;
b = RHS\LHS_b;
A = a.*(alpha_root-alpha01_2)-b.*omega;
Croot(n11);
A(1);
Cl(n11) = ( b_2^2/area_2 ) * pi * A(1);

AnA1 = zeros(NoAValues,1);
for n4 = 1:NoAValues
    AnA1(n4) = (2*n4-1)*(A(n4)/A(1))^2;
end

% Find the Local Circulation & subsequently local Cl
AnSinNTheta = zeros(NoLocations_2,NoAValues);
SumAnSinNTheta = zeros(NoLocations_2,1);
LocalCirculation = zeros(NoLocations_2,1);
LocalCl = zeros(NoLocations_2,1);
for n4 = 1:NoLocations_2
    for m1 = 1:NoAValues
        AnSinNTheta (n4,m1) = A(m1)*sin((2*m1-1)*theta(n4));
    end
    SumAnSinNTheta(n4,1) = sum(AnSinNTheta(n4,:));
    LocalCirculation(n4,1) = 2*b_2*Airspeed*SumAnSinNTheta(n4,1);
    LocalCl(n4,1) = 2*LocalCirculation(n4,1)/(Airspeed*C(n4));
    LL(n4,1) = LocalCl(n4,1) * C(n4);
end
plot(WingLocation,LocalCl)

Cdi(n11) = sum(AnA1)*pi*(b_2^2/area_2)*A(1)^2;
%DPolar = zeros(SizeTR(2),1);
Dpolar(n11,1) = Cdi(n11)/(Cl(n11)^2);
%LD =zeros(SizeTR(2),1);
LD(n11) = 1 / Dpolar(n11)*0.8;
%for n34 = 1:100
%LocalWingLoading(n34) =
   rho*Airspeed*LocalCirculation(n34);%LocalCl(n34)*C(n34);
%end
LocalCl;
%plot(WingLocation,LocalWingLoading)
Cl;
Cdi;
LD;
%waitforbuttonpress
end
plot(WingLocation,LocalCl)
%plot(TR,LD)
```

Cl

215.1. Appendix C – VEM Code (Krasny.m)

```
clear


% General constants
No_point_vertices = 400;
timestep = 0.0005;
%time = 0.01;
Scale_Factor_1 = 0.05;
Scale_Factor_2 = 0.05;
%%%%%%%%%%%%%%%%%%%%%%%%%%%%%%%%%%%%%%%%%%%%%%%%%%%%%%%%%%%%
Airspeed = 80;
% Front wing parameters
Wingspan_1 = 4;
Wing_Area_1 = 2;
Taper_Ratio_1 = 2/3;
No_Wing_Locations_1 = 500;

Zero_Lift_AOA_1 = 0;
Lift_Gradient_1 = 2*pi;
AOA_end_lin_region_1 = 12;
Stall_Angle_1 = 13;


% Rear wing parameters
Wingspan_2 = 6;
Wing_Area_2 = 4.5;
Taper_Ratio_2 = 2/3;
No_PV_2 = 2000;
No_Wing_Locations_2 = No_PV_2%/2;

Zero_Lift_AOA_2 = 0;
Lift_Gradient_2 = 2*pi;
AOA_end_lin_region_2 = 12;
Stall_Angle_2 = 13;
dx = 3;


%-----------------------------------------------------------------
% Create linear space of theta
test_theta = linspace(0,pi,2*No_point_vertices);

% Create points along wing associated with theta
PV_X = -0.5*cos(test_theta)*Wingspan_1;

% Find the midpoints of the space
for t = 2: No_point_vertices*2
    PV_X1(t-1) = 0.5*(PV_X(t-1)+PV_X(t));
end

% Find theta associated with mid points
alpha_X = acos(-2*PV_X1./Wingspan_1);
```

```
%Create initial vertical positions along origin
PV_Y = linspace(0,0,2*No_point_vertices-1);

% Create z vector in imaginary plane
z = PV_X1 + 1i*PV_Y;
z_new = linspace(0,1,2*No_point_vertices+1);


% Create time space and time when flow reaches wing
time = linspace(1,10,10);
test = size(time);
Flow_time = dx / Airspeed;
time_rear = time + Flow_time;

% Define the pitch ratev(rad/s)
pitch_rate = 1 * pi/180;

% Define the change in effective angle due to pitching moment and angle
alpha_f_dynamic = (pitch_rate * time - tan(pitch_rate*0.5*dx/Airspeed))*180/pi;
alpha_f_static = (pitch_rate * time)*180/pi;
delta_alpha_f_dynamic = pitch_rate*0.5*dx*180/pi;

% Define the y-position of rear wing
dy_dynamic = -1 *dx * sin(pitch_rate*time_rear)+ 0.5;
dy_static = -1* dx * sin(pitch_rate*time)+0.5;


for i = 1:test(2)

% dynamic run
%%%%%%%%%%%%%%%%%%%%%%%%%%%%%%%%%%%%%%%%%%%%%%%%%%%%%%%%%%%%%%%%%%%%%%%%%%%%%%%%%%%%%%%%%%%%%%%%
%%%%%%%%%%%%%%%%%%%%%%%%%%%%%%%%%%%%%%%%%%%%%%%%%%%%%%%%%%%%%%%%%%%%%%%%%%%%%%%%%%%%%%%%%%%%%%%%
%%%%%%%%%%%%%%%%%%%%%%%%%%%%%%%%%%%%%%%%%%%%%%%%%%%%%%%%%%%%%%%%%%%%%%%%%%%%%%%%%%%%%%%%%%%%%%%%
%%%%%%%%%%%%%%%%%%%%%%%%%%%%%%%%%%%%%%%%%%%%%%%%%%%%%%%%%%%%%%%%%%%%%%%%%%%%%%%%%%%%%%%%%%%%%%%%


% Assign the spanwise loading across the front wing
Vorticity = LLT_1(Wingspan_1,Wing_Area_1, Taper_Ratio_1, No_point_vertices, alpha_f_dynamic(i), Zero_Lift_AOA_1, Lift_Gradient_1, AOA_end_lin_region_1, Stall_Angle_1, Airspeed,PV_X);
for L = No_point_vertices+1 : 1 : 2* No_point_vertices
    L1 = 2*No_point_vertices+1 - L;
    Vorticity(L) = Vorticity(L1);
end
plot (PV_X,Vorticity)


for n = 1 : 1 : 1*No_point_vertices
    dis(n) = alpha_X(n+1) - alpha_X(n);
    dvort(n) = Vorticity(n+1) - Vorticity(n);
    Gi(n) = 1*dvort(n)/dis(n);
end
```

```
320.
321.for n = 1*No_point_vertices + 1 : 1 : 2*No_point_vertices -1
322.    Gi(n) = -1*Gi (2*No_point_vertices  - n );
323.end
324.
325.plot(PV_X1,Gi)
326.
327.for t = 0:timestep:Flow_time
328.    for j = 1:1:2*No_point_vertices-1
329.        for k = 1:1:2*No_point_vertices-1
330.            if j == k
331.                dzdt(j,k) = 0;
332.            else
333.                %K_sigma(j,k) = ((abs(z(j)))^2/((abs(z(j)))^2+SF^2)) -
    ((abs(z(k)))^2/((abs(z(k)))^2+SF^2));
334.                sep = z(j)-z(k);
335.                K_sigma(j,k) =
    ((abs(sep))^2)/(((abs(sep))^2)+Scale_Factor_1^2);
336.                Vort_mult (j,k) = (-1*Gi(k)/(4*1*No_point_vertices));
337.                W1(j,k)=((z(j)-z(k)))^-1;
338.                W(j,k) = (1i*(z(j)-z(k)))^-1;
339.                dzdt(j,k) = Vort_mult(j,k)*K_sigma(j,k)*W(j,k);
340.                if j < k & j > 0
341.                    dzdt(j,k) =  1 * dzdt(j,k);
342.                end
343.            end
344.        end
345.
346.        A_velocity(j) = sum(dzdt(j,:)) ;
347.        A_velocity(j) = conj(A_velocity(j));
348.        A_X (j) =  timestep * real(A_velocity(j));
349.        A_Y (j) =  timestep * imag(A_velocity(j));
350.        A_delta(j) = A_X(j) + 1i*A_Y(j);
351.        z_A(j) = z(j) + A_delta(j)*0.5;
352.
353.        for k = 1:1:2*No_point_vertices-1
354.            if j == k
355.                dzdt(j,k) = 0;
356.            else
357.                %K_sigma(j,k) = ((abs(z(j)))^2/((abs(z(j)))^2+SF^2)) -
    ((abs(z(k)))^2/((abs(z(k)))^2+SF^2));
358.                sep = z_A(j)-z(k);
359.                K_sigma(j,k) =
    ((abs(sep))^2)/(((abs(sep))^2)+Scale_Factor_1^2);
360.                Vort_mult (j,k) = (-1*Gi(k)/(4*1*No_point_vertices));
361.                W1(j,k)=((z_A(j)-z(k)))^-1;
362.                W(j,k) = (1i*(z_A(j)-z(k)))^-1;
363.                dzdt(j,k) = Vort_mult(j,k)*K_sigma(j,k)*W(j,k);
364.                if j < k & j > 0
365.                    dzdt(j,k) =  1 * dzdt(j,k);
366.                end
367.            end
368.        end
369.        B_velocity(j) = sum(dzdt(j,:)) ;
370.        B_velocity(j) = conj(B_velocity(j));
371.        B_X (j) =  timestep * real(B_velocity(j));
372.        B_Y (j) =  timestep * imag(B_velocity(j));
373.        B_delta(j) = B_X(j) + 1i*B_Y(j);
```

```
        z_B(j) = z(j) + B_delta(j)*0.5;

        for k = 1:1:2*No_point_vertices-1
            if j == k
                dzdt(j,k) = 0;
            else
                %K_sigma(j,k) = ((abs(z(j)))^2/((abs(z(j)))^2+SF^2)) -
    ((abs(z(k)))^2/((abs(z(k)))^2+SF^2));
                sep = z_B(j)-z(k);
                K_sigma(j,k) =
    ((abs(sep))^2)/(((abs(sep))^2)+Scale_Factor_1^2);
                Vort_mult (j,k) = (-1*Gi(k)/(4*1*No_point_vertices));
                W1(j,k)=((z_B(j)-z(k)))^-1;
                W(j,k) = (1i*(z_B(j)-z(k)))^-1;
                dzdt(j,k) = Vort_mult(j,k)*K_sigma(j,k)*W(j,k);
                if j < k & j > 0
                    dzdt(j,k) =  1 * dzdt(j,k);
                end
            end
        end
        C_velocity(j) = sum(dzdt(j,:)) ;
        C_velocity(j) = conj(C_velocity(j));
        C_X (j) =  timestep * real(C_velocity(j));
        C_Y (j) =  timestep * imag(C_velocity(j));
        C_delta(j) = C_X(j) + 1i*C_Y(j);
        z_C(j) = z(j) + C_delta(j)*0.5;

        for k = 1:1:2*No_point_vertices-1
            if j == k
                dzdt(j,k) = 0;
            else
                %K_sigma(j,k) = ((abs(z(j)))^2/((abs(z(j)))^2+SF^2)) -
    ((abs(z(k)))^2/((abs(z(k)))^2+SF^2));
                sep = z_C(j)-z(k);
                K_sigma(j,k) =
    ((abs(sep))^2)/(((abs(sep))^2)+Scale_Factor_1^2);
                Vort_mult (j,k) = (-1*Gi(k)/(4*1*No_point_vertices));
                W1(j,k)=((z_C(j)-z(k)))^-1;
                W(j,k) = (1i*(z_C(j)-z(k)))^-1;
                dzdt(j,k) = Vort_mult(j,k)*K_sigma(j,k)*W(j,k);
                if j < k & j > 0
                    dzdt(j,k) =  1 * dzdt(j,k);
                end
            end
        end
        D_velocity(j) = sum(dzdt(j,:)) ;
        D_velocity(j) = conj(D_velocity(j));
        D_X (j) =  timestep * real(D_velocity(j));
        D_Y (j) =  timestep * imag(D_velocity(j));
        D_delta(j) = D_X(j) + 1i*D_Y(j);

        RK_delta(j) = (A_delta(j)+2*B_delta(j)+2*C_delta(j)+D_delta(j))/6;

        PV_Xnew (j) = real(z(j)) + real(RK_delta(j));
        PV_Ynew (j) = imag(z(j)) + imag(RK_delta(j));
    end
    %subplot(1,3,1)
    plot (PV_Xnew,PV_Ynew)
```

```
    title('elements')
    %daspect([1 1 1])
    %subplot(1,3,2)
    %plot (real(z),real(velocity))
    %title('x-velocity')
    %subplot(1,3,3)
    %plot (real(z),imag(velocity))
    %title('y-velocity')
    %z = z_new;
    z = PV_Xnew + 1i*PV_Ynew;
    t
end
%%
plot (PV_Xnew,PV_Ynew)



space = zeros(1,No_PV_2);
x_pos = linspace(-0.5*Wingspan_1,0*Wingspan_2,No_PV_2+1);
y_pos = dy_dynamic(i);
for x_v = 1:1:No_PV_2+1
        space(x_v) = x_pos(x_v) +1i*y_pos;
        space_x (x_v) = x_pos(x_v);
        space_y (x_v) = y_pos;
end


for x_v = 1:1:No_PV_2+1
        for k_v = 1:1:2*No_point_vertices-1
            sep_v = space(x_v)-z(k_v);
            K_sigma_v(x_v,k_v) =
   ((abs(sep_v))^2)/(((abs(sep_v))^2)+Scale_Factor_2^2);
            Vort_mult_v(x_v,k_v) = (-1*Gi(k_v)/(4*1*No_point_vertices));
            W_v(x_v,k_v) = (1i*(space(x_v)-z(k_v)))^-1;
            dzdt_v(x_v,k_v) =
   Vort_mult_v(x_v,k_v)*K_sigma_v(x_v,k_v)*W_v(x_v,k_v);
        end
        A_velocity_v(x_v) = sum(dzdt_v(x_v,:)) ;
        A_velocity_v(x_v) = conj(A_velocity_v(x_v));
        A_X_v (x_v) =  timestep * real(A_velocity_v(x_v));
        A_Y_v (x_v) =  timestep * imag(A_velocity_v(x_v));
        A_delta_v(x_v) = A_X_v(x_v) + 1i*A_Y_v(x_v);
        space_A(x_v) = space(x_v) + A_delta_v(x_v)*0.5;

       for k_v = 1:1:2*No_point_vertices-1
            sep_v = space_A(x_v)-z(k_v);
            K_sigma_v(x_v,k_v) =
   ((abs(sep_v))^2)/(((abs(sep_v))^2)+Scale_Factor_2^2);
            Vort_mult_v(x_v,k_v) = (-1*Gi(k_v)/(4*1*No_point_vertices));
            W_v(x_v,k_v) = (1i*(space_A(x_v)-z(k_v)))^-1;
            dzdt_v(x_v,k_v) =
   Vort_mult_v(x_v,k_v)*K_sigma_v(x_v,k_v)*W_v(x_v,k_v);
        end
        B_velocity_v(x_v) = sum(dzdt_v(x_v,:)) ;
        B_velocity_v(x_v) = conj(B_velocity_v(x_v));
        B_X_v (x_v) =  timestep * real(B_velocity_v(x_v));
        B_Y_v (x_v) =  timestep * imag(B_velocity_v(x_v));
        B_delta_v(x_v) = B_X_v(x_v) + 1i*B_Y_v(x_v);
```

```
        space_B(x_v) = space(x_v) + B_delta_v(x_v)*0.5;

        for k_v = 1:1:2*No_point_vertices-1
            sep_v = space_B(x_v)-z(k_v);
            K_sigma_v(x_v,k_v) = ((abs(sep_v))^2)/(((abs(sep_v))^2)+Scale_Factor_2^2);
            Vort_mult_v(x_v,k_v) = (-1*Gi(k_v)/(4*1*No_point_vertices));
            W_v(x_v,k_v) = (1i*(space_B(x_v)-z(k_v)))^-1;
            dzdt_v(x_v,k_v) = Vort_mult_v(x_v,k_v)*K_sigma_v(x_v,k_v)*W_v(x_v,k_v);
        end
        C_velocity_v(x_v) = sum(dzdt_v(x_v,:)) ;
        C_velocity_v(x_v) = conj(C_velocity_v(x_v));
        C_X_v (x_v) =  timestep * real(C_velocity_v(x_v));
        C_Y_v (x_v) =  timestep * imag(C_velocity_v(x_v));
        C_delta_v(x_v) = C_X_v(x_v) + 1i*C_Y_v(x_v);
        space_C(x_v) = space(x_v) + C_delta_v(x_v);

        for k_v = 1:1:2*No_point_vertices-1
            sep_v = space_C(x_v)-z(k_v);
            K_sigma_v(x_v,k_v) = ((abs(sep_v))^2)/(((abs(sep_v))^2)+Scale_Factor_2^2);
            Vort_mult_v(x_v,k_v) = (-1*Gi(k_v)/(4*1*No_point_vertices));
            W_v(x_v,k_v) = (1i*(space_C(x_v)-z(k_v)))^-1;
            dzdt_v(x_v,k_v) = Vort_mult_v(x_v,k_v)*K_sigma_v(x_v,k_v)*W_v(x_v,k_v);
        end
        D_velocity_v(x_v) = sum(dzdt_v(x_v,:)) ;
        D_velocity_v(x_v) = conj(D_velocity_v(x_v));
        D_X_v (x_v) =  timestep * real(D_velocity_v(x_v));
        D_Y_v (x_v) =  timestep * imag(D_velocity_v(x_v));

        RK_U_v(x_v) = real((A_velocity_v(x_v)+2*B_velocity_v(x_v)+2*C_velocity_v(x_v)+D_velocity_v(x_v))/6);
        RK_V_v(x_v) = imag((A_velocity_v(x_v)+2*B_velocity_v(x_v)+2*C_velocity_v(x_v)+D_velocity_v(x_v))/6);
        %%%%%%%%%%%%%%%%%%%%%%%%%%%%%%%%%%%%%%%%%%%%%%%%%%%%%%%%%%%%%%%%%%%
        alpha_2(x_v) = 2 + pitch_rate*time(i) - tan((RK_V_v(x_v)-delta_alpha_f_dynamic)/Airspeed);
end

CL_rear_dynamic(i) = LLT_2_twist(Wingspan_2, Wing_Area_2, Taper_Ratio_2, No_PV_2, alpha_2, Zero_Lift_AOA_2, Airspeed, x_pos*1.5 );

%%%%%%%%%%%%%%%%%%%%%%%%%%%%%%%%%%%%%%%%%%%%%%%%%%%%%%%%%%%%%%%%%%%%%%%%%%%%%%%%%%%%%%%%%%%%%%%%%%%%
%%%%%%%%%%%%%%%%%%%%%%%%%%%%%%%%%%%%%%%%%%%%%%%%%%%%%%%%%%%%%%%%%%%%%%%%%%%%%%%%%%%%%%%%%%%%%%%%%%%%
%%%%%%%%%%%%%%%%%%%%%%%%%%%%%%%%%%%%%%%%%%%%%%%%%%%%%%%%%%%%%%%%%%%%%%%%%%%%%%%%%%%%%%%%%%%%%%%%%%%%
%%%%%%%%%%%%%%%%%%%%%%%%%%%%%%%%%%%%%%%%%%%%%%%%%%%%%%%%%%%%%%%%%%%%%%%%%%%%%%%%%%%%%%%%%%%%%%%%%%%%


% static run
```

```
%%%%%%%%%%%%%%%%%%%%%%%%%%%%%%%%%%%%%%%%%%%%%%%%%%%%%%%%%%%%%%%%%%%%%%%%%%%%%%%%%%%%%%%%%%%%%%%%
%%%%%%%%%%%%%%%%%%%%%%%%%%%%%%%%%%%%%%%%%%%%%%%%%%%%%%%%%%%%%%%%%%%%%%%%%%%%%%%%%%%%%%%%%%%%%%%%
%%%%%%%%%%%%%%%%%%%%%%%%%%%%%%%%%%%%%%%%%%%%%%%%%%%%%%%%%%%%%%%%%%%%%%%%%%%%%%%%%%%%%%%%%%%%%%%%
%%%%%%%%%%%%%%%%%%%%%%%%%%%%%%%%%%%%%%%%%%%%%%%%%%%%%%%%%%%%%%%%%%%%%%%%%%%%%%%%%%%%%%%%%%%%%%%%


% Assign the spanwise loading across the front wing
Vorticity = LLT_1(Wingspan_1,Wing_Area_1, Taper_Ratio_1, No_point_vertices, alpha_f_static(i), Zero_Lift_AOA_1, Lift_Gradient_1, AOA_end_lin_region_1, Stall_Angle_1, Airspeed,PV_X);
for L = No_point_vertices+1 : 1 : 2* No_point_vertices
    L1 = 2*No_point_vertices+1 - L;
    Vorticity(L) = Vorticity(L1);
end
plot (PV_X,Vorticity)


for n = 1 : 1 : 1*No_point_vertices
    dis(n) = alpha_X(n+1) - alpha_X(n);
    dvort(n) = Vorticity(n+1) - Vorticity(n);
    Gi(n) = 1*dvort(n)/dis(n);
end

for n = 1*No_point_vertices + 1 : 1 : 2*No_point_vertices -1
    Gi(n) = -1*Gi (2*No_point_vertices  - n );
end

plot(PV_X1,Gi)

for t = 0:timestep:Flow_time
    for j = 1:1:2*No_point_vertices-1
        for k = 1:1:2*No_point_vertices-1
            if j == k
                dzdt(j,k) = 0;
            else
                %K_sigma(j,k) = ((abs(z(j)))^2/((abs(z(j)))^2+SF^2)) - ((abs(z(k)))^2/((abs(z(k)))^2+SF^2));
                sep = z(j)-z(k);
                K_sigma(j,k) = ((abs(sep))^2)/(((abs(sep))^2)+Scale_Factor_1^2);
                Vort_mult (j,k) = (-1*Gi(k)/(4*1*No_point_vertices));
                W1(j,k)=((z(j)-z(k)))^-1;
                W(j,k) = (1i*(z(j)-z(k)))^-1;
                dzdt(j,k) = Vort_mult(j,k)*K_sigma(j,k)*W(j,k);
                if j < k & j > 0
                    dzdt(j,k) =  1 * dzdt(j,k);
                end
            end
        end

        A_velocity(j) = sum(dzdt(j,:)) ;
        A_velocity(j) = conj(A_velocity(j));
        A_X (j) =  timestep * real(A_velocity(j));
        A_Y (j) =  timestep * imag(A_velocity(j));
```

```
        A_delta(j) = A_X(j) + 1i*A_Y(j);
        z_A(j) = z(j) + A_delta(j)*0.5;

        for k = 1:1:2*No_point_vertices-1
            if j == k
                dzdt(j,k) = 0;
            else
                %K_sigma(j,k) = ((abs(z(j)))^2/((abs(z(j)))^2+SF^2)) -
    ((abs(z(k)))^2/((abs(z(k)))^2+SF^2));
                sep = z_A(j)-z(k);
                K_sigma(j,k) =
    ((abs(sep))^2)/(((abs(sep))^2)+Scale_Factor_1^2);
                Vort_mult (j,k) = (-1*Gi(k)/(4*1*No_point_vertices));
                W1(j,k)=((z_A(j)-z(k)))^-1;
                W(j,k) = (1i*(z_A(j)-z(k)))^-1;
                dzdt(j,k) = Vort_mult(j,k)*K_sigma(j,k)*W(j,k);
                if j < k & j > 0
                    dzdt(j,k) =  1 * dzdt(j,k);
                end
            end
        end
        B_velocity(j) = sum(dzdt(j,:)) ;
        B_velocity(j) = conj(B_velocity(j));
        B_X (j) =  timestep * real(B_velocity(j));
        B_Y (j) =  timestep * imag(B_velocity(j));
        B_delta(j) = B_X(j) + 1i*B_Y(j);
        z_B(j) = z(j) + B_delta(j)*0.5;

        for k = 1:1:2*No_point_vertices-1
            if j == k
                dzdt(j,k) = 0;
            else
                %K_sigma(j,k) = ((abs(z(j)))^2/((abs(z(j)))^2+SF^2)) -
    ((abs(z(k)))^2/((abs(z(k)))^2+SF^2));
                sep = z_B(j)-z(k);
                K_sigma(j,k) =
    ((abs(sep))^2)/(((abs(sep))^2)+Scale_Factor_1^2);
                Vort_mult (j,k) = (-1*Gi(k)/(4*1*No_point_vertices));
                W1(j,k)=((z_B(j)-z(k)))^-1;
                W(j,k) = (1i*(z_B(j)-z(k)))^-1;
                dzdt(j,k) = Vort_mult(j,k)*K_sigma(j,k)*W(j,k);
                if j < k & j > 0
                    dzdt(j,k) =  1 * dzdt(j,k);
                end
            end
        end
        C_velocity(j) = sum(dzdt(j,:)) ;
        C_velocity(j) = conj(C_velocity(j));
        C_X (j) =  timestep * real(C_velocity(j));
        C_Y (j) =  timestep * imag(C_velocity(j));
        C_delta(j) = C_X(j) + 1i*C_Y(j);
        z_C(j) = z(j) + C_delta(j)*0.5;

        for k = 1:1:2*No_point_vertices-1
            if j == k
                dzdt(j,k) = 0;
            else
```

```
                %K_sigma(j,k) = ((abs(z(j)))^2/((abs(z(j)))^2+SF^2)) -
    ((abs(z(k)))^2/((abs(z(k)))^2+SF^2));
                sep = z_C(j)-z(k);
                K_sigma(j,k) =
    ((abs(sep))^2)/(((abs(sep))^2)+Scale_Factor_1^2);
                Vort_mult (j,k) = (-1*Gi(k)/(4*1*No_point_vertices));
                W1(j,k)=((z_C(j)-z(k)))^-1;
                W(j,k) = (1i*(z_C(j)-z(k)))^-1;
                dzdt(j,k) = Vort_mult(j,k)*K_sigma(j,k)*W(j,k);
                if j < k & j > 0
                    dzdt(j,k) =  1 * dzdt(j,k);
                end
            end
        end
        D_velocity(j) = sum(dzdt(j,:)) ;
        D_velocity(j) = conj(D_velocity(j));
        D_X (j) =  timestep * real(D_velocity(j));
        D_Y (j) =  timestep * imag(D_velocity(j));
        D_delta(j) = D_X(j) + 1i*D_Y(j);

        RK_delta(j) = (A_delta(j)+2*B_delta(j)+2*C_delta(j)+D_delta(j))/6;

        PV_Xnew (j) = real(z(j)) + real(RK_delta(j));
        PV_Ynew (j) = imag(z(j)) + imag(RK_delta(j));
    end
    %subplot(1,3,1)
    plot (PV_Xnew,PV_Ynew)
    title('elements')
    %daspect([1 1 1])
    %subplot(1,3,2)
    %plot (real(z),real(velocity))
    %title('x-velocity')
    %subplot(1,3,3)
    %plot (real(z),imag(velocity))
    %title('y-velocity')
    %z = z_new;
    z = PV_Xnew + 1i*PV_Ynew;
    t
end
%%
plot (PV_Xnew,PV_Ynew)


space = zeros(1,No_PV_2);
x_pos = linspace(-0.5*Wingspan_1,0*Wingspan_2,No_PV_2+1);
y_pos = dy_static(i);
for x_v = 1:1:No_PV_2+1
        space(x_v) = x_pos(x_v) +1i*y_pos;
        space_x (x_v) = x_pos(x_v);
        space_y (x_v) = y_pos;
end


for x_v = 1:1:No_PV_2+1
        for k_v = 1:1:2*No_point_vertices-1
            sep_v = space(x_v)-z(k_v);
```

```
            K_sigma_v(x_v,k_v) =
    ((abs(sep_v))^2)/(((abs(sep_v))^2)+Scale_Factor_2^2);
            Vort_mult_v(x_v,k_v) = (-1*Gi(k_v)/(4*1*No_point_vertices));
            W_v(x_v,k_v) = (1i*(space(x_v)-z(k_v)))^-1;
            dzdt_v(x_v,k_v) =
    Vort_mult_v(x_v,k_v)*K_sigma_v(x_v,k_v)*W_v(x_v,k_v);
        end
        A_velocity_v(x_v) = sum(dzdt_v(x_v,:)) ;
        A_velocity_v(x_v) = conj(A_velocity_v(x_v));
        A_X_v (x_v) =  timestep * real(A_velocity_v(x_v));
        A_Y_v (x_v) =  timestep * imag(A_velocity_v(x_v));
        A_delta_v(x_v) = A_X_v(x_v) + 1i*A_Y_v(x_v);
        space_A(x_v) = space(x_v) + A_delta_v(x_v)*0.5;

       for k_v = 1:1:2*No_point_vertices-1
            sep_v = space_A(x_v)-z(k_v);
            K_sigma_v(x_v,k_v) =
    ((abs(sep_v))^2)/(((abs(sep_v))^2)+Scale_Factor_2^2);
            Vort_mult_v(x_v,k_v) = (-1*Gi(k_v)/(4*1*No_point_vertices));
            W_v(x_v,k_v) = (1i*(space_A(x_v)-z(k_v)))^-1;
            dzdt_v(x_v,k_v) =
    Vort_mult_v(x_v,k_v)*K_sigma_v(x_v,k_v)*W_v(x_v,k_v);
        end
        B_velocity_v(x_v) = sum(dzdt_v(x_v,:)) ;
        B_velocity_v(x_v) = conj(B_velocity_v(x_v));
        B_X_v (x_v) =  timestep * real(B_velocity_v(x_v));
        B_Y_v (x_v) =  timestep * imag(B_velocity_v(x_v));
        B_delta_v(x_v) = B_X_v(x_v) + 1i*B_Y_v(x_v);
        space_B(x_v) = space(x_v) + B_delta_v(x_v)*0.5;

        for k_v = 1:1:2*No_point_vertices-1
            sep_v = space_B(x_v)-z(k_v);
            K_sigma_v(x_v,k_v) =
    ((abs(sep_v))^2)/(((abs(sep_v))^2)+Scale_Factor_2^2);
            Vort_mult_v(x_v,k_v) = (-1*Gi(k_v)/(4*1*No_point_vertices));
            W_v(x_v,k_v) = (1i*(space_B(x_v)-z(k_v)))^-1;
            dzdt_v(x_v,k_v) =
    Vort_mult_v(x_v,k_v)*K_sigma_v(x_v,k_v)*W_v(x_v,k_v);
        end
        C_velocity_v(x_v) = sum(dzdt_v(x_v,:)) ;
        C_velocity_v(x_v) = conj(C_velocity_v(x_v));
        C_X_v (x_v) =  timestep * real(C_velocity_v(x_v));
        C_Y_v (x_v) =  timestep * imag(C_velocity_v(x_v));
        C_delta_v(x_v) = C_X_v(x_v) + 1i*C_Y_v(x_v);
        space_C(x_v) = space(x_v) + C_delta_v(x_v);

        for k_v = 1:1:2*No_point_vertices-1
            sep_v = space_C(x_v)-z(k_v);
            K_sigma_v(x_v,k_v) =
    ((abs(sep_v))^2)/(((abs(sep_v))^2)+Scale_Factor_2^2);
            Vort_mult_v(x_v,k_v) = (-1*Gi(k_v)/(4*1*No_point_vertices));
            W_v(x_v,k_v) = (1i*(space_C(x_v)-z(k_v)))^-1;
            dzdt_v(x_v,k_v) =
    Vort_mult_v(x_v,k_v)*K_sigma_v(x_v,k_v)*W_v(x_v,k_v);
        end
        D_velocity_v(x_v) = sum(dzdt_v(x_v,:)) ;
        D_velocity_v(x_v) = conj(D_velocity_v(x_v));
        D_X_v (x_v) =  timestep * real(D_velocity_v(x_v));
```

```
        D_Y_v (x_v) =  timestep * imag(D_velocity_v(x_v));

        RK_U_v(x_v) =
real((A_velocity_v(x_v)+2*B_velocity_v(x_v)+2*C_velocity_v(x_v)+D_velocity_
v(x_v))/6);
        RK_V_v(x_v) =
imag((A_velocity_v(x_v)+2*B_velocity_v(x_v)+2*C_velocity_v(x_v)+D_velocity_
v(x_v))/6);
        %%%%%%%%%%%%%%%%%%%%%%%%%%%%%%%%%%%%%%%%%%%%%%%%%%%%%%%%%%%%%%%%%%%%
        alpha_2(x_v) = 2 + pitch_rate*time(i) -
tan((RK_V_v(x_v))/Airspeed);
end

CL_rear_static(i) = LLT_2_twist(Wingspan_2, Wing_Area_2, Taper_Ratio_2,
No_PV_2, alpha_2, Zero_Lift_AOA_2, Airspeed, x_pos*1.5 );


%%%%%%%%%%%%%%%%%%%%%%%%%%%%%%%%%%%%%%%%%%%%%%%%%%%%%%%%%%%%%%%%%%%%%%%%%%%%
%%%%%%%%%%%%%%%%%%%%%%%%%%%%%%%%%%%%%%%%%%%%%%%%%%%%%%%%%%%%%%%%%%%%%%%%%%%%
%%%%%%%%%%%%%%%%%%%%%%%%%%%%%%%%%%%%%%%%%%%%%%%%%%%%%%%%%%%%%%%%%%%%%%%%%%%%
%%%%%%%%%%%%%%%%%%%%%%%%%%%%%%%%%%%%%%%%%%%%%%%%%%%%%%%%%%%%%%%%%%%%%%%%%%%%

% No Front Wing
%%%%%%%%%%%%%%%%%%%%%%%%%%%%%%%%%%%%%%%%%%%%%%%%%%%%%%%%%%%%%%%%%%%%%%%%%%%%
%%%%%%%%%%%%%%%%%%%%%%%%%%%%%%%%%%%%%%%%%%%%%%%%%%%%%%%%%%%%%%%%%%%%%%%%%%%%
CL_rear_nf(i) = LLT_1_rear(Wingspan_2, Wing_Area_2, Taper_Ratio_2, No_PV_2,
alpha_f_static(i)+2, Zero_Lift_AOA_2, Airspeed, x_pos*1.5 );
%%%%%%%%%%%%%%%%%%%%%%%%%%%%%%%%%%%%%%%%%%%%%%%%%%%%%%%%%%%%%%%%%%%%%%%%%%%%
%%%%%%%%%%%%%%%%%%%%%%%%%%%%%%%%%%%%%%%%%%%%%%%%%%%%%%%%%%%%%%%%%%%%%%%%%%%%

end


plot(time, CL_rear_dynamic, 'k-', 'LineWidth', 1)
hold on
plot(time, CL_rear_static, 'k--', 'LineWidth', 1)
%plot(time, CL_rear_nf, 'k-.', 'LineWidth', 1)
hold off
ylabel("Rear Wing Total Lift Lift Coefficient")
xlabel("Time (s)")
legend('Dynamic', 'Static')
```